EXPERIMENTAL INVESTIGATION OF AN ARC HEATER

Thesis by

Marc L. Renard

In Partial Fulfillment of the Requirements

For the Degree of

Aeronautical Engineer

California Institute of Technology

Pasadena, California

1962

ACKNOWLEDGMENTS

The author wishes to express his deep gratitude to Professor Toshi Kubota, under whose expert guidance this work was carried out and to whom he is indebted for numerous precious advice and hours of fruitful discussion, and to Professors Lees and Zukoski, members of his supervising committee. He acknowledges the help provided by the hypersonic laboratory staff in the installation of some experimental devices, and by the GALCIT 10 foot tunnel staff in the computations. Thanks are extended to Mrs. G. Van Gieson for typing the manuscript, and to Mrs. N. Kindig and Mr. J. Van Dijk for preparing the figures.

For their generosity and constant solicitude, special appreciation is expressed to the members of the Executive Committee and the Secretaries, in New York and Brussels, of the Belgian-American Educational Foundation, by whom the author was appointed a C. R. B. Graduate Fellow for 1960-1961.

ABSTRACT

An electric arc heater, intended to provide a steady flow of high stagnation temperature gas (up to 10,000°K) into a convergent-divergent nozzle, was designed at the GALCIT Hypersonic Laboratory.

Section 2 first gives a few preliminary calculations which have been made for the arc heater-nozzle combination, using argon, at stagnation pressures of 1 and 2 atm., and assuming equilibrium flow. In particular, the Mach number in the test section of a fixed nozzle will depend on the thermodynamic properties at the reservoir.

In the heater, the direct-current arc is axially constricted by a channel parallel to the gas flow. A description of the design and instrumentation is given in Sections 2 and 3.

For two series of experiments, using argon, the central electrode was either the cathode, as in the conventional arrangement, or the anode: both configurations were thoroughly investigated. Provided a sharp edge exists at the end of the flow constricting channel, the configuration with anode in the center was found to give, generally, a more stable functioning, with a voltage drop about twice as large, higher efficiency and thus higher average temperature for the same mass flow of gas, as compared to the case where the cathode is in the center. In the ranges of power (up to 13 Kw) and mass flow (up to 6.00 gr/sec) investigated, it was found that the best efficiency is obtained for a swirl close to the central electrode and large gas mass flows. When the anode is in the center, a long and narrow constricting channel leads to the optimal conditions. With the reversed polarities, the geometry of the downstream

channel is not very important.

Finally, a tentative explanation of the results is given, emphasizing in particular that the "anode in the center" case corresponds to a "long" arc, and the "cathode in the center" to a "short" one with poorer transfer of energy from the arc to the gas.

TABLE OF CONTENTS

PART		PAGE
	Acknowledgments	ii
	Abstract	iii
	Table of Contents	v
	List of Symbols	vi
1.	The Arc Heater	1
2.	Design of Arc Heater	2
	2.1. Preliminary Calculations	2
	2.2. Design of Arc Heater	6
3.	Preliminary Tests	11
	3.1. Tests A-7 and S-1	11
	3.2. Influence on the Injection Angle on the Performance of the Heater	14
	3.3. Conclusions from Preliminary Experiments	16
4.	Systematic Study of Efficiency, Arc Characteristics in the Arc Heater as Functions of Geometry, Polarity, and Mass Flow Parameters	18
	4.1. Introduction	18
	4.2. Experimental Set-Up	18
	4.3. Variables of the Problem and Experimental Results	18
	4.4. Tentative Interpretation of Physical Results	25
5.	General Conclusions	31
	References	33
	Appendix -- Equilibrium Speed of Sound in Ionizing Argon	34
	Tables	37
	Figures	47

LIST OF SYMBOLS

a	adiabatic speed of sound
A	cross-section of the channel, or of the nozzle
c	specific heat
d	distance from central electrode tip to exit section
d'	distance from central electrode tip to inner shoulder of arc chamber
e	heat of ionization
E	electric field
f( )	function of
h	specific enthalpy (K. M. S.)
H	total specific enthalpy (K. M. S.)
I	electric current in the arc
K	constant of law of mass action
ℓ	depending on the case, distance from central electrode tip to exit section, or length of constricting channel; or heat of reaction, or liter
$\dot{m}$ or m'	mass flow of gas (in gr/sec), or water (in liter/sec)
$\mathcal{M}$	mass flow of gas per unit area of constricting channel
n	newton
p	pressure
P	power, or heat added per second in the heater
$\mathcal{S}$	reduced net power input into the gas per unit area of throat section
R	gas constant of argon
s	specific entropy (K. M. S.)
T	absolute temperature

u	velocity along axis of the channel
v	velocity of the flow, or specific volume
V	voltage drop
x	abscissa along axis of the channel, or of the nozzle
α	degree of ionization
γ	ratio of specific heats
η	efficiency of energy transfer process
θ	ratio of absolute temperature to ionization temperature
ρ	density of gas
ϕ	diameter of constricting channel
> +	central electrode positive
> -	central electrode negative

Superscripts

*	sonic condition
-	average

Subscripts

A	of argon
+	of the ion
e	at equilibrium; or of the electron
g	of the gas
i	of ionization
o	at $0^{\circ}K$, or at $0^{\circ}C$
t	stagnation condition

1. THE ARC HEATER

During the last few years, arc heating devices have been studied and used for many technical purposes connected with missile and space technology. They generate steady flows of gas at stagnation temperatures of thousands of degrees Kelvin, which are needed, among others[1, 2], in the following applications:

(1) convergent-divergent expansion in a nozzle to achieve high velocities in the test section with high free stream temperatures for study of heat transfer and ablation rates (moderate reservoir pressure); or high velocities in the test section with low free stream temperatures for aerodynamic heating (high reservoir pressure).

(2) Supply of hot gases at high pressure and temperature for hypersonic wind tunnels.

(3) Magnetohydrodynamic studies.

(4) Low thrust propulsion devices.

(5) Study of flow of weakly ionized gases.

This work deals with the design and experimental study of the performance of a direct-current arc heater of the axial type, which means that the gas to be heated flows along a circular channel parallel to the path of the arc (Figure 1). The working fluid is argon at atmospheric pressure with a settling chamber and Laval nozzle connected to the exit section. The heater will be used to generate steady supersonic flows of high static temperatures.

It has to be stressed that there does not seem to be any reason to reject, a priori, the positive central electrode configuration, as has been done by previous workers.

2. DESIGN OF ARC HEATER

2.1. Preliminary Calculations

In order to obtain an estimate of various physical quantities occuring in the arc heater (Figure 1), and the nozzle flow, some preliminary calculations are made based on the one-dimensional flow of gases at very high temperatures.

For one-dimensional steady flows of a frictionless gas, at thermodynamic equilibrium, we have:

Continuity Equation:

$$\frac{d\rho}{\rho} + \frac{du}{u} + \frac{dA}{A} = 0 \quad , \quad \text{or} \quad \rho u A = \text{constant} = \dot{m} \tag{1}$$

Momentum Equation:

$$\rho u \, du + dp = 0 \tag{2}$$

Energy Equation:

$$d\left(h + \tfrac{1}{2} u^2 \right) = \frac{dP}{\dot{m}} \tag{3}$$

Equation of State:

$$p = p(\rho , h) \tag{4}$$

Here p, ρ, h, u are the pressure, density, specific enthalpy and velocity of the gas, and A is the cross-sectional area of the channel, which is supposed to be given as a function of the distance along the channel, x. dP is the heat added to the gas per unit time. The heats of dissociation and ionization are not included in dP, but they are a part of the enthalpy h. Thus dP is not zero only in the heater. Define the

stagnation enthalpy H, as

$$H = \tfrac{1}{2} u^2 + h \quad . \tag{5}$$

Then

$$\dot{m}\, d\, H = dP \tag{6}$$

in the heater and

$$d\, H = 0 \tag{7}$$

elsewhere. By combining Eqs. 2 and 3, we obtain

$$\dot{m}\, T\, d\, s = d\, P \quad , \tag{8}$$

where s is the specific entropy , T the temperature. Thus the flow is isentropic outside the heater.* For the isentropic flow,

$$(dp/d\rho) = a_e^2 \tag{9}$$

where a_e is the speed of sound at thermodynamic equilibrium. Then eliminating p and ρ between Eqs. 1, 2, and 9, we obtain

$$\frac{dA}{A} = \left(\frac{u^2}{a_e^2} - 1 \right) \frac{du}{u} \quad . \tag{10}$$

Thus A is minimum at $u = a_e$, or $M_e = \frac{u}{a_e} = 1$. The total mass flow rate through the channel is given by

$$\dot{m} = \rho_e^* a_e^* A^* \quad , \tag{11}$$

as in the perfect gas case. Also, from Eq. 7

$$H = h + \tfrac{1}{2} u^2 = \text{constant} = h_t \quad . \tag{12}$$

---

* This is valid only for equilibrium flow or frozen flow. When the chemical reaction goes on at a finite rate, the entropy increases.

Hence the flow properties in a Laval nozzle are determined once the stagnation condition is given. For example, the stagnation condition can be specified by the pressure p_t and the enthalpy h_t. Then the corresponding entropy is obtained as s_t, and the flow properties are determined as functions of h:

$$\begin{aligned} p &= p(h, s_t) \\ \rho &= \rho(h, s_t) \\ u &= \sqrt{2(h_t - h)} \end{aligned} \tag{13}$$

The pressure and density of the gas is most easily obtained graphically on the Mollier chart of the working gas. a_e may be computed as indicated in the Appendix, with the assumption of the perfect gas behaviour for the atoms, the ions and the electrons individually, which is consistent with the method used to compute the Mollier chart[2]. The sonic condition is determined at the point where u = a. Then the area ratio A/A^* is obtained from $A/A^* = \rho^* a^*_e / \rho u$.

Across the heater,

$$h_t - H_{in} = (1/\dot{m})\, P \quad , \tag{14}$$

where H_{in} is the stagnation enthalpy of the incoming gas, h_t the stagnation enthalpy of the exhaust gas, P the total power transferred to the gas. For practical purpose, H_{in} is equal to the static enthalpy of the incoming gas, since its Mach number is very small. For a given nozzle, the total mass flow rate is a function of h_t and p_t,

$$\dot{m} = \dot{m}(h_t, p_t) \quad . \tag{15}$$

Thus when p_t and P are given, $\dot{m}$ and h_t are determined by Eqs. 14 and 15.

Eq. 15 may also be used to estimate h_t from the measurement of $\dot{m}$ and p_t .

Table 1 gives the mass flow per unit area of the throat, $\rho^* a^*$, as a function of the reduced stagnation enthalpy for the two reservoir pressures p_t = 1 atm. and 2 atm.

In Figure 2, we plotted $\rho^* a^*$, as a function of h_t/RT_o for the two pressures: p_t = 1 atm. and 2 atm. The dotted curves represent the same relation for the perfect, non-ionized gas of constant c_p[4].

On the same figure, curves of $\rho^* a^*$ for constant $\mathcal{P} = \frac{P}{RT_o A^*}$ have been drawn; they vary like $\frac{1}{h_t/RT_o}$, while $\rho^* a^*$ for p_t = constant, vary like $\frac{1}{\sqrt{h_t/RT_o}}$ in the region of the perfect gas. The use of these curves is illustrated in the following numerical example.

Numerical Example

Supposing the efficiency and the gross power input are known

Given $P = 20$ Kw

and $m' = 1.235$ gr/sec

p_t = 1 atm.,

then,

from Eq. 14: $(h_t/RT_o) = 285$.

on Figure 2, the curve for p_t = 1 atm. yields for $(h_t/RT_o) = 285$,

$\rho^* a^* = 35.5$ kgmass/m^2 . sec

Hence: $A^* = 0.348$ cm.^{2}

(1) What is the new mass flow in the above nozzle if we double the reservoir pressure (p_t = 2 atm.), and the net power input (P= 40 Kw)? Then

$\mathcal{F}$ = 20,000 (kgmass/m^2 sec.).

The curve $\mathcal{F}$ = 20,000 intersects the mass-flow curve for p_t = 2 atm. at the point (h_t/RT_o) = 274, $\rho^* a^*$ = 72.75. Hence, the mass flow with the nozzle A^* = 0.348 cm^2 and p_t = 2 atm. is

m' = 2.53 gr/sec

(2) With the same nozzle and the same P = 20 Kw, what is the new mass flow if we double the reservoir pressure (p_t = 2 atm.)?

Since, $\mathcal{F}$ = 10,000, the point of the intersection of $\mathcal{F}$ = 10,000 with p_t = 2 atm. yields:

(h_t/RT_o) = 107

$\rho^* a^*$ = 93.25 :

Thus, m' = 3.25 gr/sec.

2.2. Design of Arc Heater

The arc heater is essentially made out of an arc-chamber, properly shaped, through which argon flows and is heated and eventually ionized.

It can be divided into four parts: the insulated head, the arc-chamber itself, the outer electrode cooling system, the anode and anode cooler (Figure 1).

2. 2. 1. Description and Design of Generator Blocks

2. 2. 1. 1. The Insulated Head and Distributor

The head is cylindrical and made out of micarta; it can be fixed by six nuts to the copper arc chamber. In its center is a hole which, with the one through the distributor disk, provides a smooth friction passage for the movable cylindrical electrode.

When the removable disk, d, is pushed into its seat, a small chamber remains, into which the gas is brought, through hole h. The gas then flows through injectors with an exit hole drilled normal to the axis. The gas can be injected into the arc-chamber with any degree of rotation, from 0^{o} (radial injection) to 90^{o} (tangential injection) by adjusting the orientation of injectors (Figure 3).

2. 2. 1. 2. Arc-Chamber

The arc-chamber itself is machined from a copper block. It has a cylindrical chamber, a conical contraction section and a cylindrical arc constricting section. The arc will strike the outer electrode somewhere along the cylindrical water-cooled constricting channel.

2. 2. 1. 3. Central Electrode

The central copper electrode is $\frac{1}{2}$" in diameter and is rounded at its end. It goes through the insulated head and the distributor disk, and is blocked at a minimum distance of 1/4" from the shoulder in the arc-chamber.

The cooling system is composed of a copper tube (1/4" in diameter) inside the electrode, which is the water inlet; the space between

the inner and outer tubes provides the outlet.

2. 2. 2. Auxiliary Set-Ups

2. 2. 2. 1. Electrodes

The central electrode is adjustable inside the chamber to position the electrode distance for stable arc operation; this is accomplished manually with a lever clamped on the central electrode.

The electrical power lead is connected to a copper block clamped around the tube; this provides the necessary good contact over a sufficient surface.

The other lead is connected to the copper frame which supports the arc-chamber.

2. 2. 2. 2. Arc Starter

For conservation of the electrodes, the arc cannot be started by bringing into contact and moving away the central and the outer electrode. Instead, it was decided to use the exploding wire technique to start the arc. A very thin piano wire is introduced into the chamber through a tiny hole, along which a sufficient contact with the wire is assured. It is held in position through a strongly compressed teflon piece; the latter prevents also any leakage. The switch-on current makes the wire melt instantaneously and creates a local overheating and ionization, which enables the principal arc to start (Figure 5).

2.2.2.3. Water Connections

At the central electrode, the water goes through the inner tube. At the outer electrode, the incoming water flows first around the terminal part of the constricting channel.

2.2.3. Instrumentation

Since the purpose of the experiment is to determine the efficiency of the energy transfer process to argon through the arc, the instrumentation described below was provided. The set-up is illustrated clearly by the diagram of Figure 6.

2.2.3.1. Water Cooling Circuits

Two flowmeters, thoroughly calibrated, measure respectively the total flow through the central and outer electrodes, and the flow through the central electrode. The arc-chamber flow is determined by difference.

To fix an order of magnitude of the water flows involved, a preliminary test gave:

central: $m' = 0.1252\ \ell$/sec.

outer: $m' = 0.166\ \ell$/sec.

The inlet and outlet temperatures, for both electrodes, are measured by thermopiles (copper-constantan), placed in micarta blocks at the inlets and outlets; the readings being made on a Leeds Northrup K-2 potentiometer. To isolate the thermopiles electrically from the electrodes, water connections between the block and the electrodes were made out of plastic tubing and a short length of copper tubing at

the micarta block end, the latter being electrically grounded.

2.2.3.2. Gas Circuit

A Fisher and Porter Triflat flowmeter, with a stainless steel ball float, was used to measure the mass flow of argon. Its calibration curve was computed for 2 upstream pressures: 50 and 60 psi. A pressure gage measures the pressure in the arc chamber.

2.2.3.3. Electric Circuit

The electric power input was measured by reading:

$-V_{arc}$, voltage drop across the arc

$-I_{arc}$, arc current .

The stabilization resistance was kept at 2.9 ohms. In the range of power, 0 - 13 Kw, the current could be adjusted by regulation of the output voltage of the D. C. generators.

3. PRELIMINARY TESTS

3.1. Tests A-7 and S-1

From the first two tests on the arc heater, we were able to draw some qualitative conclusions and, therefrom, were induced to modify some experimental devices in order to obtain significant results.

The details of the instrumentation and some characteristic results are recorded in Table 2.

The efficiency of the energy transfer process to the gas is defined by the ratio of the power added to the gas, P_{gas} to the power dissipated in the arc, P_{input}:

$$\eta = \frac{P_{gas}}{P_{input}} \quad .$$

P_{gas} is measured by an energy balance

$$P_{gas} = P_{input} - P_{electrodes} \quad ,$$

where $P_{electrodes}$ is the power absorbed by the cooling circuit. It is determined by careful measurements of the water mass flow and the temperature rise through the electrodes circuit. P_{input} is simply the product of the voltage drop across the arc V_{arc} by the arc current I_{arc}. Direct reading of the two last quantities enables the arc characteristic to be drawn. Thus

$$\eta = 1 - \frac{P_{electrodes}}{P_{input}} \quad .$$

Finally, the average temperature of the gas, $\overline{T}_g$, can be obtained from Figure 7, which gives $\overline{T}_g$ as a function of the net power input per unit

mass flow (P_{gas}/m') or ($\eta P_{input}/m'$).

In these first two tests, we used the block described in the previous section. However, the thermometric measurements in the water-cooling circuit were made with a Brown self-balancing potentiometer and single non-grounded iron-constantan thermocouples. Owing to the smallness of the difference in temperatures involved it appeared that any hope for accuracy was somewhat illusory. Only some orders of magnitude and qualitative conclusions could be obtained.

The gas was injected with an angle of 90^{o} (Figure 3) in both cases, and the distance d (Figure 5) was varied around a position (about 1 diameter from the inner shoulder) which gave enough stability without excessive overheating of the electrodes. The power level and the mass flow were kept at moderate values (not exceeding 4 Kw and 1.4 gr/sec). The pressure in the chamber was seen to be atmospheric within a very few per cent.

The most striking fact revealed by experience is the complete difference in behaviour of the arc with different polarities for identical geometry, angle of injection and mass flow.

When the central electrode is positive (A-7), the arc turns out to be fairly stable, even with copper electrodes. It undoubtedly strikes the cathode along the sharp edge XX (Figure 5), where, after a few minutes, an intense erosion occurs. Once the copper in XX is burning, one observes appreciable fluctuations of voltage drop across the arc and of brilliancy, the burned copper giving a green color to the jet. No damage is seen on the central electrode (anode). To avoid this erosion, one thinks at first to suppress the concentration of field in XX

by rounding off the sharp edge. But, as will appear more clearly at the end of the next section, the existence of a sharp edge at the exit section is precisely essential to that functioning with anode in the center: when the damaged part was rounded off, the arc became completely unstable, and blew itself off even with such a large starting voltage as 200 V. Since in conventional designs[2, 6], the conical part of the arc chamber is already the convergent part of the nozzle, followed by the throat and the divergent section having no sharp edge, this could presumably explain why the "anode in the center" was found an unstable configuration, and previous experimentators only retained the "cathode in the center" case.

The efficiency, varying from 50 per cent to 70 per cent, was of the same order of magnitude as in Cann's data[1].

With that polarity, the voltage drop, of about 50 V, is found to be insensitive to the distance d, but the arc quickly becomes more unstable, the more d is increased.

When the central electrode is negative (S-1), the arc is more unstable, in current as well as in voltage. This will be seen in all our experiments. Furthermore, the central electrode, made out of copper, is readily damaged: the arc strikes the cathode around the center of the tip, digging a crater and projecting drops of copper in the flow. Furthermore, the fact that XX was not damaged at all, that a very slight erosion was seen on the inner shoulder and that the arc looked as being "inside" gave a first experimental evidence that the arc was striking along the "short" path going from the tip of the central electrode to the wall of the arc-chamber, which is what occurs in the conventional

polarity configuration[2, 6]. Accordingly, the voltage drop across the arc (about 30 V) was reduced by a factor of the order of 2. At this stage, no measurements of efficiency were made. However, with that reduced voltage drop and small heating region, one should expect the efficiency to be smaller, which is indeed the case. Finally, V_{arc} is seen to increase slightly with increasing d.

Tests A-7 and S-1 stress the necessity for very heat-resistant electrodes and more accurate measurements of the temperature increase of the cooling water. The latter is a twofold requirement: in sensitivity of the reading; and in appropriate insulation of the thermocouple, which is introduced in the water circuit, while the water itself is in contact with conducting parts of the electric circuit.

Hence we modified the set-up as described in Section 2.2.

In the succeeding tests, a ring of 2 per cent thoriated tungsten was put at the exit section (Figure 8), to prevent the sharp edge XX from being damaged by the arc striking. It was not eroded in the course of experiment. Eventually, the whole tube of the constricting channel was made out of tungsten, but this turned out to be a useless precaution. Thoriated tungsten was used also for the 60°-conically shaped central electrode tip (Figure 9).

3.2. Influence of the Injection Angle on the Performance of the Heater

The tests reported in Table 2 (S-11; S-22; S-26; O-11; O-12), the results of which are given on Figures 11 to 13 , consisted essentially of measuring, by the method described at the beginning of this section, the efficiency of the energy transfer process into the gas and in obtaining

the arc characteristic for:

(1) various "degrees" of swirl (variation of the direction of the injection velocity: See Figure 3)

(2) for a fixed degree of injection, various mass flows

(3) for a fixed mass flow, various values of the current or, subsequently, of the gross power input (P_{input})

(4) the two configurations: "anode in the center", noted > + ; "cathode in the center" noted > - .

As previously, the pressure in the arc chamber was very slightly above atmospheric pressure. The distance d from the tip of the central electrode to the exit section was kept constant at around 2 inches when the anode is in the center, at 1.6 inches in the opposite case. These distances gave stable functioning points over the whole range of power investigated. As to the injection angle, the main feature is that, with radially injected gas, the arc is very unstable, and leads to poor efficiencies: in the worst case (cathode in the center), an excessive overheating of the distributor could be seen. With a 90^{o} or 45^{o} angle of injection, the arc is very stable. As could be expected, the 45^{o} injection gives slightly better results than the 90^{o} one, since the first angle corresponds to jets very close to the central electrode (Figure 3), while, for the second one, the gas stream collides against the walls of the chamber.

Regarding the influence of the other factors on the efficiency and arc characteristic, a quantitative confirmation of the higher efficiency and voltage drop, when the anode is in the center, was obtained, as well as their evolution with increasing mass flow and power input.

In the experimental data of Figures 11 to 13, when the electrodes were allowed to reach their equilibrium temperature, the results were reproducible within one point of efficiency.

3.3. Conclusions from Preliminary Experiments

By observing the experimental data and by comparing them, several conclusions can be drawn, which will guide us in further systematic study of the efficiency. It can be stated:

(1) Whatever the polarity, the efficiency decreases with increasing gross power input, for given injection and mass flow; the efficiency increases with increasing mass flow, for given injection and power input. It is optimum for 45^{o} injection (slightly better, more constant than 90^{o}). The 0^{o} injection (radial) has to be rejected.

(2) For the efficiency, the "positive central electrode" configuration is much more advantageous, all other factors being equal.

(3) Whatever the polarity, V_{arc} is nearly constant, or increases slowly with increasing currents, for given injection angle and mass flow. It shifted upwards, a few volts or less, with increasing mass flow (0.92 to 1.98 gr/sec), for given injection angle. It decreased very slightly with increasing angle of injection above 45^{o}, for given mass flow.

(4) The "positive central electrode" configuration presents a voltage drop which is on the average of about 40 V, while the cathode central electrode configuration gives only 25 V. Consequently, it seems that the first case will be more advantageous for maximizing the transfer to the arc.

(5) As to the average gas temperature, for given mass flow and power input, $\overline{T}_g$ being a monotonously increasing function of the ratio $\frac{\eta P_{input}}{m'}$, varies like η ; but for increasing m', the effect of (1/m') in the ratio is much stronger than the corresponding increase in efficiency, so that $\overline{T}_g$ decreases.

4. SYSTEMATIC STUDY OF EFFICIENCY AND ARC CHARACTERISTICS IN THE ARC HEATER AS FUNCTIONS OF GEOMETRY, POLARITY, AND MASS FLOW PARAMETERS

4.1. Introduction

The purpose of this experimental study was to proceed to an investigation of the influence, on the efficiency and arc characteristic, of various parameters of geometry and mass flow, for gross power input up to 13 Kw.

4.2. Experimental Set-Up

It is fundamentally the same as the one described before: the same central electrode with tungsten tip, the micarta head and gas distributor were kept; it should be noted that the angle of injection was kept at the fixed value 45°, which previous experiments have proved sufficiently to give the optimum efficiency, all other factors being held constant.

A copper block, with 30° inclined walls and an exit section of $\emptyset = \frac{1}{2}''$, provided the arc-chamber, fixed to the micarta head (Figure 1). To this block, various removable constriction sections can be adapted (Figure 10). The tube forming the walls of the last section, where the arc most likely strikes, is of tungsten instead of copper.

4.3. Variables of the Problem and Experimental Results

The dependent variables of the problem are as before:

the efficiency, $\eta = \frac{P_{gas}}{P_{input}}$, and the voltage drop across the arc,

V_{arc}.

They are functions of:

(1) The ratio, ℓ/ϕ, of the length of the arc constricting channel to the diameter of its section;

(2) The diameter, ϕ, of the constricting channel;

(3) The magnitude of the mass flow m';

(4) The polarities: central electrode positive being noted > +

central electrode negative being noted > - ;

(5) The power input.

The position of the central electrode, given by d' on Figure 10, is not a parameter: it was chosen equal to $\frac{1}{2}$", by a compromise between the necessity for a stable arc (arc unstable for large d', especially for > -), and for not overheating the electrodes if brought too close together, or shortening the arc excessively.

An interesting compound parameter in the problem is the mass flow per unit area of the cross section of the outer electrode. We define a "mass factor": $\mathcal{M}$ = (m'/A), where

m' = mass flow of gas, in gr/sec

A = $\pi (\phi^2/4)$ = area of cross section, in inches^2 .

$\mathcal{M}$ is in some sense the "image" of the velocity through the circular channel (proportional to the exit velocity, if ρ_{exit} was constant). Having in mind the example, of say, pneumatic circuit-breakers, we may predict that above some critical value of $\mathcal{M}$, the arc will not be maintained in a stable position, or will just be blown away. The latter occurs for $\mathcal{M}$ = 122, the polarity > + , and the "long" arc ℓ/ϕ = 8 , whatever the starting voltage up to 250V.

4.3.1. Particular Values Chosen

(1) for ϕ: $\frac{1}{2}$, 0.354, 1/4 (inches) giving sections,

$$\text{with } A = \frac{\pi(1/4)^2}{4} \text{ inches}^2 \quad ,$$

4A 2A A

(2) For l/ϕ 1 2 4 8

(3) Polarities: > + and > -

(4) Values of m': 6, 4.24, 3, 2.12, 1.50, 1.06 (gr/sec)

Values of $\mathcal{M}$ are multiples of each other. They vary between 5.4 and 122 gr/sec x inches^2.

Table 4 gives a listing of the experiments performed, with their index number, which for clarity is omitted on the corresponding graphs.

4.3.2. Experimental Results

Experimental results are given graphically in Figures 14 to 29. For compactness, no curves have been drawn here; but the conclusions which follow are based on separate graphs plotted for each case.

Each figure corresponds to one value of l/ϕ (in decreasing order), one polarity (> + before > -), and various mass flows and diameters; in each case are reported $\eta = f(P_{input})$ and $V_{arc} = f(I_{arc})$.

Furthermore, for a typical example of variation of these quantities with l only, all other factors being constant, the reader should refer to Figure 30 and Figures 32 to 35.

The maximum and minimum values obtained in the whole set of experiments are recorded below. It emphasizes the fact that very large

changes in η , V_{arc} are obtained when changing the polarities, mass flow and geometry; furthermore, extremal values of these quantities appear, if not always very pronounced, for extremal values of the parameters.

A. Arc Voltage, V_{arc}

I. > + : Central Electrode Positive

(a) Maximum Value

V = 150.5 V at 63A; P_{input} = 9,482 w;
η = 84 per cent; $\overline{T}_g$ = 3,650°K; m' = 4.24 gr/sec;
$\mathcal{H}$ = 86.4; ℓ/ϕ = 4 ; ϕ = 1/4" .

The voltage drop was observed to be greater for ℓ/ϕ = 8 ; ϕ = 1/4" , but was unstable.

(b) Minimum Value

V_{arc} = 26.5 V at 140.5 A ; P_{input} = 5,710 W; η = 44.2 per cent
$\overline{T}_g$ = 2,950°K ; m' = 1.06 gr/sec ; $\mathcal{H}$ = 5.4; ℓ/ϕ = 1 , ϕ = $\frac{1}{2}$"

II. > - : Central Electrode Negative

(a) Maximum Value

V_{arc} = 79.75 V at 148A (11,803 w); η = 62 per cent ;
$\overline{T}_g$ = 2,300°K; m' = 5.00 gr/sec; $\mathcal{H}$ = 122.24; ℓ/ϕ = 8, ϕ = 1/4"

(b) Absolute Minimum Values

V_{arc} = 18.25 V at 143.5A ; P_{input} = 2,942 W ;

η = 25.6 per cent; $\overline{T}_g$ = 1,820°K ; m' = 1.06 gr/sec;

$\mathcal{H}$ = 10.8; ℓ/ϕ = 1 ; ϕ = 0.354" (same result for ϕ = 1/4")

B. Efficiency

I. > + : Central Electrode Positive

(a) Maximum

η = 87.9 per cent ; P_{input} = 8,200 w ;

V_{arc} = 132.25 V ; I = 62 A ; $\overline{T}_g$ = 1,430°K ; m' = 3.00 gr/sec;

$\mathcal{H}$ = 61.12 (equivalent results for $\mathcal{H}$ = 86.4 ; $\mathcal{H}$ = 122.4 could not be obtained, the arc blowing itself off)

(b) Minimum

η = 41.0 per cent ; P_{input} = 1.831 W ; V_{arc} = 28 V ;

I = 186A ; $\overline{T}_g$ = 3,830°K ; m' = 1.06 gr/sec; $\mathcal{H}$ = 5.4 .

II. > - : Central Electrode Negative

(a) Maximum

η = 83.7 per cent ; P_{input} = 5,372 W ; V_{arc} = 79 V ;

I = 68A ; $\overline{T}_g$ = 1,500°K ; m' = 6.00 gr/sec ; $\mathcal{H}$ = 122.24 ;

ℓ/ϕ = 2 and ϕ = 1/4" (ℓ/ϕ = 1 was not experimented)

(b) Minimum

η = 14.7 per cent ; P_{input} = 3.608 W ; V_{arc} = 20.5 V;

I = 176A ; $\overline{T}_g$ = 980°K ; m' = 1.06 gr/sec; $\mathcal{M}$ = 5.4 ;

ℓ/ϕ = 8 ; $\phi = \frac{1}{2}$"

4.3.3. Conclusions

At least in the range of variation of the different quantities, the results of the experiments show the choice of the parameters to be made in order to get the best η , largest V_{arc} and highest $\overline{T}_g$. (See Table 4.)

A first condition for high efficiency is, as stated before, an injection with a swirl close to the central electrode.

The comparison of the two polarity cases: > + (central electrode positive) and > - (central electrode negative) clearly proves that for best η , V_{arc} , $\overline{T}_g$, > + has to be preferred to > - .

Whatever the polarity, one must take the largest possible values of the mass flow per unit area $\mathcal{M}$ (Thus: large mass flows and small diameters of the constriction section), but always considering the need for a stable arc (See Section 4.3.) and sufficient temperatures at the exit. Large values of ℓ have to be chosen for optimum efficiency and large voltage drop when the anode is in the center (> +); small values of ℓ with the reversed polarities (> -). The reason for that difference will be seen in what follows.

Now, after analyzing the experimental data, it was possible to

summarize, as is done synthetically in Table 4, the influence of the various parameters on η and V_{arc}. This table outlines the general trend of the variables with the variation of the parameters, to which a very few exceptions may exist (in particular, jumps in position, and thus in voltage drop, can occur for the short arc).

Some further comments have to be made. First, experiments confirm what is expected intuitively: that the efficiency and the voltage drop vary together in the same sense. Paragraph 4 of this section gives evidence that an important voltage drop occurs in the positive column of the arc, at least in the case > + : so, the larger the voltage drop, the larger the ionization and heating region, and the larger the efficiency.

As stated above, for given geometry and mass flow, the efficiency is seen to be better when the anode is in the center for the same power input, and the voltage is higher by a factor of about 2, for the same current.

The configuration > + is much more stable, in general, than > - . This difference in behavior does not appear clearly at high mass flow, and can even be reversed at very high values of $\mathcal{M}$. For the configuration > + , (dV/dI) is positive, while for the second one, (dV/dI) is negative for moderate currents, and eventually slightly positive for very high currents.

For both polarities, efficiency and voltage drop decrease with the power input, in general, increase with increasing mass flow and decreasing diameter, and always increase with increasing $\mathcal{M}$. It can be remarked that for the configuration > - , V_{arc} increases slightly

with increasing diameter at small mass flows, which was attributed to a local overheating and choking at small diameters, causing a "thermal" drop in voltage; while at large mass flows, V_{arc} goes down with the diameter because the increased flow speed sweeps the arc downstream. Finally, in the central-electrode-positive > + configuration, the efficiency and arc voltage go up with the length ℓ, which corresponds closely to the length of the arc, and thus the heating region. In the > - configuration, the arc does not extend over the whole length of constricting section, and ℓ is just a useless length of "cooling channel", so that η should indeed decrease with ℓ, while V_{arc} remains constant.

4.4. Tentative Interpretation of Physical Results

4.4.1. Physical Model

In the static case, the potential distribution in the electric arc is represented by Figure 4, giving V = V(x), x being the distance "along" the arc. Since the regions where the cathode and anode voltage drop occurs are small, the length of the positive column can be equated, with negligible error, to the total length of the arc.

We distinguish three regions:

(1) Cathode-drop region, of very high positive ion-space density, with V_c "large". V_c may be taken, at atmospheric pressure, as the first ionization potential = 15.76 V.

(2) Positive column, where E is constant and depends on the nature of the gas, the pressure and the current. The voltage drop in the positive column is then proportional to the length of the arc.

(3) Anode-drop region, of very high electron-space density,

with V_a smaller than V_c .

To that physical situation, we superimpose a flow pattern of which we consider only the axial effects (along the axis of the column) on the electric phenomena: we call the effects of the flow "mechanical".

We are now trying to define roughly the degree of the coupling between the "electrical" and "mechanical" flows. Accordingly, we compare the ion- and electron- drift velocities to the flow velocity.

(1) The average conditions considered are

$\overline{T}$ = 3,000°K , p = 1 atm; m' = 3.00 gr/sec; ϕ = 0.354 inches.

Plotting $V_{arc} = f(\ell)$ for I = 100 A , p = 1 atm, we find

$$\frac{dV_{arc}}{d\ell} = \text{constant} = \overline{E} = 10 \text{ V/cm.}$$

The ion drift velocity is[5]:

$\overline{v}_+ = K_+ \overline{E}$, and $K_+ = \frac{e L}{m \overline{c}}$. Then

$\overline{v}_+ = 45.5$ cm/sec.

The electron drift velocity is

$$\overline{v}_e = K_e \overline{E}$$

By Compton's formula[5]:

$$K_e = \frac{271,000 \ \lambda_{10} \ (273/T)^{\frac{1}{2}}}{\left\{1 + \left[1 + 1,106,000 \ M \lambda_{10}^{\ 2} \ (E/p)^2\right]^{\frac{1}{2}}\right\}^{\frac{1}{2}}}$$

where

λ_{10} = electron mean free path at 1 mm Hg., 273°K

M = molecular weight of the gas

$\overline{E}$ = electric field in V/cm

p = pressure in mm Hg

Thus $\bar{v}_e = 133,350$ cm/sec.

The "flow velocity" is the average velocity in the constricting channel:

$$\bar{v}_{flow} = 28,460 \text{ cm/sec.}$$

The velocity ratios of the flow on the ions and electrons are respectively

$$\frac{\bar{v}_{flow}}{\bar{v}_+} = 626 \quad \text{while} \quad \frac{\bar{v}_{flow}}{\bar{v}_e} = 0.2135 \quad ,$$

and one should then expect the ions to be strongly affected by the flow, and the electrons very little.

(2) In the general case, when one does not assume any particular value for $\bar{v}$, $\bar{\rho}$, S, $\bar{T}$, $\bar{E}$, one writes

$$\frac{\bar{v}_{flow}}{\bar{v}_+} = \frac{1}{\bar{E}} \quad \frac{m'/\bar{\rho} S}{e / m \bar{c}} \quad .$$

Since

$$\bar{c} \div \sqrt{\bar{T}} \quad , \quad \lambda \div \frac{1}{\rho} \quad ,$$

$$\frac{\bar{v}_{flow}}{\bar{v}_+} = \text{constant} \quad . \quad \frac{\mathcal{M}}{\bar{E}} \sqrt{\bar{T}} \quad ,$$

so that it can be stated that the action of the flow on the ions will be increased with

increasing $\mathcal{M}$ (large mass flow or/and small diameter)

increasing temperature $\bar{T}$

decreasing field .

On the other hand, if in the computation of $\bar{v}_e$ by Compton's formula, 1 is neglected compared to about 10, then $\bar{v}_e \sim \frac{1}{\sqrt{\bar{E}}}$, so

that

$$\frac{\bar{v}_{flow}}{\bar{v}_e} = \text{constant} \cdot \frac{\mathcal{M}}{\sqrt{\bar{E}}} \bar{T} \quad .$$

Hence, fixing $\bar{v}_{flow}$, the relative importance of the "electronic" and "ionic" behavior of the arc is estimated by

$$\frac{\bar{v}_e}{\bar{v}_+} = \text{constant} \frac{1}{\sqrt{\bar{E}\ \bar{T}}} \quad .$$

4.4.2. Comparison of "Central Electrode Positive" and "Central Electrode Negative" Functionings

A schematic representation of the "central electrode positive" and "central electrode negative" configurations can be found in Figure 31. In the flow field, there are three possible regions of concentration of the electric field: A, central cathode tip; B, inner shoulder; C, exit section edge.

A. "Central Electrode Positive" Configuration

It can be argued that the arc will strike along either AB (from the tip to the inner shoulder) or AC (from the tip to the exit section edge). Because of the strong coupling between flow and ions, the ions can easily be carried downstream in the direction of their own drift velocity, while the electrons going upstream do not "see the flow".* One should then expect a strong electric field, and thus voltage drop, in order to

---

* This was sufficiently proved experimentally: the inner shoulder remaining sharp, the edge of the exit section had been rounded off. In the "central electrode positive" configuration, the arc could not be maintained for any value of the current.

maintain the arc attached to the edge C. The anode-drop of the electrons, furthermore, occurring in a "dead-water" region of the flow should be small. From what has been said in the preceding paragraph, one can predict quantitatively:

the larger $\mathcal{M}$, the larger becomes the voltage drop, and

for very large velocities, the arc is blown away, whatever the starting field.

If V_a , V_c are taken as constant, increasing the length ℓ results in a corresponding increase of the voltage drop in the positive column, so that

$$V_{total} = V_{an} + V_{cath} + \left(\frac{d\, V_{total}}{d\, \ell} \right) \ell$$

B. "Central Electrode Negative" Configuration

The ions, strongly affected by the mechanical action of the flow, this time have a small drift velocity directed upstream of the flow. It seems probable that they will take the shortest path BA from the inner shoulder to the central electrode tip of the order of $\frac{1}{2}$"("short" arc configuration). The voltage drop at the cathode now occurs in the "dead-water" region of the flow where the motion of the ions is easier: hence a smaller average voltage drop. Furthermore, this causes the "ionic" character of the discharge to be less important: $\bar{v}_{flow}/\bar{v}_{+}$ should decrease, which for constant $\mathcal{M}$ implies

$\bar{T}$ larger, improbable, since the flow does not stay long enough in the heating region;

$\bar{E}$ large, which effectively is the case. (Of the order of 23 V/cm).

Finally, the efficiency should drop with ℓ , the region downstream

of B being a useless "cooling channel". The voltage drop across the arc must increase with $\mathcal{M}$ and depends on the downstream geometry only through the influence of ϕ on the velocities around the inner shoulder B, and not through ℓ . This point will be checked now.

C. Voltage Drop in the Positive Column

In order to check the validity of the above representation, we plotted $V_{arc} = f(\ell)$, ℓ being the length of the positive column, for a given value of the polarity, the diameter, the mass flow, and the current (Figures 32 to 35). For the "central electrode positive" configuration, $V_{arc} = f(\ell)$ is indeed linear, which justifies a posteriori the assumptions: V_a , V_c constant and $V_{arc} = V_{total} = V_{an} + V_{cath} + \overline{E}\ell$, where $\overline{E}$ = constant = $(dV/d\ell)$. $\overline{E}$ is seen to increase strongly with increasing $\mathcal{M}$, but for high values of $\mathcal{M}$ and I , the arc is not maintained. For the "central electrode negative" configuration, $V_{arc} = f(\ell)$ is practically constant, which shows that the length of the positive column does not vary with the length of the constricting channel: indeed, the arc, striking along the "short" path is unaffected by what is downstream.

5. GENERAL CONCLUSIONS

This study determines the influence of the various geometric parameters, mass flow, and polarity on the efficiency of an arc heater of the axial type at low power level.

Provided a sharp edge exists at the exit section of the constricting channel, the "central electrode positive" configuration gives better results in any respect, except that the "long" arc is blown away more easily for large values of the mass flow per unit area. It was found in particular that the efficiency and the voltage drop across the heater are always larger, compared to the case where the cathode is in the center.

When the central electrode is positive, the efficiency is seen to increase slightly with the length of the constricting channel, and to increase with increasing mass flow per unit area $\mathcal{M}$. With increasing $\mathcal{M}$, the voltage drop increases strongly, and it varies linearly, with a large slope, with the length of the channel ("long" arc configuration). Furthermore, it increases with increasing current ("positive" arc characteristic).

When the central electrode is negative, the efficiency decreases for longer channels and increases with $\mathcal{M}$. The voltage drop increases with $\mathcal{M}$, remains unaffected by the length of the downstream channel ("short" arc configuration), and decreases with increasing current ("negative" arc characteristic). However, further investigation is needed to check whether significant changes in behaviour could not occur if the arc is forced, mechanically and/or electrically, to strike

further downstream.

The above investigation stresses the advantage of having the anode in the center, a swirl close to the central electrode, and a long and narrow constricting channel, which presumably is completely filled by the plasma of the positive column.

REFERENCES

1. Cann, Gordon L.: Energy Transfer Processes in a Partially Ionized Gas. GALCIT Hypersonic Research Project, Memorandum No. 61, June 15, 1961.

2. Westinghouse Electric Corporation: Description of Arc Heater System. Arc Heater Symposium of the Westinghouse Electric Corporation, East Pittsburgh, Pennsylvania, September, 1960.

3. Cann, Gordon L.: Mollier Chart for Argon. Plasmadyne Corporation, Santa Ana, California, Air Force Office of Scientific Research, Contract No. AF 49(638)-54, February 20, 1959.

4. Mueller, James N.: Equations, Tables and Figures for Use in the Analysis of Helium Flow at Supersonic and Hypersonic Speeds. NACA Technical Note 4063, September, 1957.

5. Cobine, James D.: Gaseous Conductors. Dover Publications, Inc., New York, N. Y., 1958.

6. Clayden, W. A.: Recent Research in the ARDE Low Density Wind Tunnel with a Plasma Jet Heater. Rarefied Gas Dynamics, edited by L. Talbot, p. 715, Academic Press, New York, N. Y., 1961.

APPENDIX

EQUILIBRIUM SPEED OF SOUND IN IONIZING ARGON

The equilibrium speed of sound in ionizing argon is calculated with the assumptions:

(1) single degree of ionization

(2) perfect-gas equations for argon atoms, ions, and electrons.

If α denotes the degree of ionization, i.e., the mass fraction of argon ions, the equation of state of the mixture of atoms, ions and electrons may be written as

$$p = (1 + \alpha)\, \rho\, R\, T \tag{A.1}$$

where R is the gas constant of the argon atom, and the enthalpy is given by

$$\begin{aligned} h &= h_A + (2h_{A+} - h_A)\, \alpha \\ &= 5/2 \quad RT - e_o + (\ 5/2 \quad RT + e_o\ )\, \alpha \quad , \end{aligned} \tag{A.2}$$

where e_o is the heat of ionization per unit mass at 0^oK. From the thermodynamic formulas, it can be shown that

$$a_e^2 = (\partial p/\partial \rho)_s = \frac{c_p}{c_p\, (\partial \rho/\partial p)_T - (T/\rho^2)\, (\partial \rho/\partial T)_p^2} \tag{A.3}$$

Calculating c_p, $(\partial \rho/\partial p)_T$ and $(\partial \rho/\partial T)_p$ from Eqs. A.1 and A.2 and substituting in Eq. A.3, we obtain, with $a_o^2 = 5/3\ \gamma\ p/\rho$,

$$\left(\frac{a_e}{a_o}\right)^2 = \frac{1 + \left(1 + \frac{2}{5}\frac{e_o}{RT}\right)\frac{T}{1+a}\left(\frac{\partial a}{\partial T}\right)_p}{1 - \frac{5}{3}\frac{p}{1+a}\left(\frac{\partial a}{\partial p}\right)_T + \frac{1}{3}\left(1 + 2\frac{e_o}{RT}\right)\frac{T}{1+a}\left(\frac{\partial a}{\partial T}\right)_p - \frac{5}{3}\left[\ \ldots\ldots\right.} \qquad \text{(A. 4)}$$

$$\left. \ldots\ldots \left(1 + \frac{2}{5}\frac{e_o}{RT}\right)\frac{p}{1+a}\left(\frac{\partial a}{\partial p}\right)_T - \frac{2}{5}\frac{T}{1+a}\left(\frac{\partial a}{\partial T}\right)_p\right]\frac{T}{1+a}\left(\frac{\partial a}{\partial T}\right)_p \quad .$$

Applying the law of mass action to the ionization of argon, we obtain

$$\frac{a^2}{1-a^2} = \frac{K(T)}{p} \quad . \qquad \text{(A. 5)}$$

From the reciprocity relations of thermodynamics we have

$$(\partial h/\partial p)_T = v - T\,(\partial v/\partial T)_p \quad . \qquad \text{(A. 5)}$$

From Eq. A. 2, we obtain the relation

$$(\partial h/\partial p)_T = \ell_I\,(\partial a/\partial p)_T \quad , \qquad \text{(A. 7)}$$

where $\ell_I = 2h_{A_+} - h_A$.

From Eqs. A. 1, A. 6, and A. 7, we obtain

$$\ell_I\,(\partial a/\partial p)_T = -\frac{R_3 T^2}{p}\,(\partial a/\partial T)_p \quad . \qquad \text{(A. 8)}$$

Computing $(\partial a/\partial p)_T$ and $(\partial a/\partial T)_p$ from Eq. A. 5, substituting in Eq. A. 8, yields

$$\frac{1}{K}\frac{dK}{dt} = \frac{\ell_I}{RT^2} = \frac{5}{2}\frac{1}{T} + \frac{e_o}{RT^2} \quad ,$$

and

$$K = \text{constant} \cdot T^{5/2} \exp\left(-\frac{e_o}{RT}\right) \quad .$$

Hence, we obtain

$$(\partial a/\partial T)_p = \left(5/2 + \frac{e_o}{RT} \right) \frac{a(1-a^2)}{2T}$$
$$(\partial a/\partial p)_T = - \frac{(1-a^2)}{2p} \quad a \quad , \tag{A. 9}$$

which, introduced in Eq. A. 4, give

$$\left(\frac{a_e}{a_o}\right)^2 = \frac{\theta^2 + \frac{5}{4} \left(\frac{2}{5} + \theta \right)^2 a (1 - a)}{\theta^2 + \frac{5}{12}\left[2\theta^2 + (\theta + \frac{2}{5})(\theta+2)\right]a(1-a) + \frac{25}{12} (\theta + \frac{2}{5})^2 a^2 (1-a)^2} \tag{A. 10}$$

where $\theta = (T/\theta_i)$ and $\theta_i \equiv (e_o/R) = 182.9 \times 10^3$ °K for argon.

In Eq. A. 10, θ being very small, a small, terms of order $\theta^2 a$ can be neglected. Finally:

$$\left(\frac{a_e}{a_o}\right)^2 = \frac{\theta^2 + \frac{1}{5} (1 + 5\theta) a (1 - a)}{\theta^2 + \frac{1}{3} (1 + 3\theta) a (1-a) + \frac{1}{3} (1 + 5 \theta) a^2 (1 - a)^2} \quad . \tag{A. 11}$$

TABLE 1

GAS PROPERTIES AT SONIC CONDITION

Remarks: (1) a_e computed by the formulas of the Appendix
(2) a_e neglected under 10^{-3}

Reference: Mollier Chart for Argon[2]

1. p_t = 1 atm

Dim.	Point / Quant.	1	2	3	4	5	6	7	8	9
^oK	T_t	14,000	12,000	11,000	10,000	8,000	6,000	5,000	4,000	3,000
-	a_t	0.4	0.115	0.053	0.022	0.0015	~0	~0	~0	~0
-	h_t/RT_o	445	199	141	107	74	54	45	37	27
$\frac{m}{sec}$	$v^*=a_e^*$	1,885	1,670	1,605	1,590	1,470	1,250	1,140	1,020	883
-	h^*/RT_o	414	174.6	118.4	84.7	55	54	45	37	27
$\frac{n}{m^2}$	p^*	59.7×10^3	59.6×10^3	54.5×10^3	52×10^3	47×10^3	49.4×10^3	49.4×10^3	49.4×10^3	49.4×10^3
^oK	T^*	13,460	11,340	10,180	8,680	6,100	4,500	3,750	3,000	2,250
-	a^*	0.37	0.0906	0.0328	0.0049	~0	~0	~0	~0	~0
$\frac{kgmass}{m^3}$	ρ^*	0.01553	0.0231	0.0249	0.0286	0.037	0.0527	0.0633	0.0790	0.0820
$\frac{kgmass}{m^2.sec}$	ρ^*a^*	29.3	38.6	40.0	45.5	54.3	65.9	72.2	80.6	93

TABLE 1 (CONTINUED)

2. p_t = 2 atm

Dim.	Point / Quant.	1	2	3	4	5	6	7
^oK	T_t	14,000	12,000	11,000	9,000	6,000	5,000	4,000
-	a_t	0.2918	0.082	0.037	0.033	~0	~0	~0
-	h_t/RT_o	358	175	129	86	54	45	37
$\frac{m}{sec}$	$v^*=a_e^*$	1,828	1,680	1,682	1,535	1,250	1,140	1,020
-	$h-/RT_o$	328.6	150.4	104	64.5	54	45	37
$\frac{n}{m^2}$	p^*	$130x10^3$	$117.2x10^3$	104	102	$98.8x10^3$	$98.8x10^3$	$98.8x10^3$
^oK	T^*	13,405	11,290	9,880	7,050	4,500	3,750	3,000
-	a^*	0.2675	0.0609	0.0184	~0	~0	~0	~0
$\frac{kgmass}{m^3}$	ρ^*	0.03672	0.047	0.0497	0.0695	0.1054	0.1266	0.158
$\frac{kgmass}{m^2.sec}$	ρ^*a^*	67.1	78.5	84.0	108.7	131.8	144.4	161.2

TABLE 2

SUMMARY OF PRELIMINARY EXPERIMENTS

Remark: In connection with Section 4, it is mentioned that the tests described below correspond to a geometry: d' (Figure 10) = 0.43"; $\phi = \frac{1}{2}$"; $\ell/\phi = 3.14$

Pressure in chamber: 1 atm $\overset{+}{\sim}$ 0.2 psi

Test	Injection Angle	Electrodes	Electrode Distance* (in)	V_{arc}; Variation with d	Gas Mass Flow(gr/sec)	Power Input (max.)	Efficiency	V_{arc} (volts)	I_{arc} (amp)	Remarks
A-7	90°	> +	1-7/8	Insensitive to d, except for stability	1.4	4 kw	50~70%	45~50	70~130	Electrodes copper - copper; arc fairly stable
S-1	90°	> -	1-3/4 2	Increases slightly with d	1.4	2.4 kw	--	50~60	25~60	Electrodes copper - copper arc unstable
S-11	90°	> +	2	Figure 11 and 13	0.92~1.98	8 kw	42~72	33~46	50~180	Electrodes: >+ copper ; >-thoriated tungsten ring
S-22	0°	> +	2	11 and 13	0.92~1.98	8 kw	30~68	36~46	50~170	Electrodes: see S-11
S-26	0°	> +	2	11 and 13	0.92~1.98	8 kw	55~75	35~48	40~180	Electrodes: see S-11

* From tip of central electrode to exit section

TABLE 2 (CONTINUED)

Test	Injection Angle	Electrodes	Electrode Distance* (in)	Figure	Gas Mass Flow(gr/sec)	Power Input (max.)	Efficiency	V_{arc} (volts)	I_{arc} (amp)	Remarks
O-11	90°	> -	1.57	12 and 13	0.92~1.98	4.5 kw	35~45	22~26	40~190	Electrodes: >+ with tungsten tip (Fig. 9), >- with tungsten tube
O-12	45°	> -	1.57	12 and 13	0.92~1.98	4.5 kw	37~50	22~26	40~190	Electrodes: See O-11

* From tip of central electrode to exit section

TABLE 3

EXPERIMENTS PERFORMED

m'(gr/sec)			Values of $\dot{m}_e$ (gr/sec x inches^2)					
ϕ(inches)			6.00	4.24	3.00	2.12	1.50	1.06
1/2	$\ell/\phi = 8$	> +	30.56 N-22, I	21.6 N-22, II	15.28 N-22, III	10.8 O-27, I	7.64 O-27, II	5.4 O-27, III
		> -	30.56 N-22, IV	21.6 N-22, V	15.28 N-22, VI	10.8 O-27, IV	7.64 O-27, V	5.4 O-27, VI
	$\ell/\phi = 4$	> +				10.8 O-25, I	7.64 O-25, II	5.4 O-25, III
		> -				10.8 O-25, IV	7.64 O-25, V	5.4 O-25, VI
	$\ell/\phi = 2$	> +	30.56 N-26, I	21.6 N-26, II	15.28 N-26, III	10.8 O-20, I	7.64 O-20, II	5.4 O-20, III
		> -	30.56 N-26, IV	21.6 N-26, V	15.28 N-26, VII	10.8 O-20, IV	7.64 O-20, V	5.4 O-20, VI
	$\ell/\phi = 1$	> +				10.8 O-29, I	7.64 O-29, II	5.4 O-29, III
		> -				10.8 O-29, IV	7.64 O-29, V	5.4 O-29, VI

TABLE 3 (CONTINUED)

m'(gr/sec) / ϕ(inches)			Values of $\mathcal{H}$ (gr/sec x inches^2)					
			6.00	4.24	3.00	2.12	1.50	1.06
0.354	$\ell/\phi = 8$	> +	61.12 N-20, I	43.2 N-20, II	30.56 N-20, III	21.6 N-7, I	15.28 N-7, II	10.8 N-7, III
		> -	61.12 N-20, IV	43.2 N-20, V	30.56 N-20, VI	21.6 N-7, IV	15.28 N-7, V	10.8 N-7, VI
	$\ell/\phi = 4$	> +				21.6 N-8, I	15.28 N-8, II	10.8 N-8, III
		> -				21.6 N-8, IV	15.28 N-8, V	10.8 N-8, VI
	$\ell/\phi = 2$	> +	61.12 N-21, I	43.2 N-21, II	30.56 N-21, III	21.6 N-9, I	15.28 N-9, II	10.8 N-9, III
		> -	61.12 N-21, IV	43.2 N-21, V	30.56 N-21, VI	21.6 N-9, IV	15.28 N-9, V	10.8 N-9, VI
	$\ell/\phi = 1$	> +				21.6 N-10, I	15.28 N-10, II	10.8 N-10, III
		> -				21.6 N-10, IV	15.28 N-10, V	10.8 N-10, VI

TABLE 3 (CONTINUED)

m'(gr/sec)			Values of $\mathcal{H}$ (gr/sec x inches^2)					
			6.00	4.24	3.00	2.12	1.50	1.06
ϕ(inches)								
1/4	$\ell/\phi = 8$	> +	122.24 N-19, I	86.4 N-19, II	61.12 N-19, III	43.2 N-11, I	30.56 N-11, II	21.6 N-11, III
		> -	122.24 N-19, IV	86.4 N-19, V	61.12 N-19, VI	43.2 N-11, IV	30.56 N-11, V	21.6 N-11, VI
	$\ell/\phi = 4$	> +				43.2 N-2, I	30.56 N-2, II	21.6 N-2, III
		> -				43.2 N-2, IV	30.56 N-2, V	21.6 N-2, VI
	$\ell/\phi = 2$	> +	122.24 N-18, I	86.4 N-18, II	61.12 N-18, III	43.2 N-14, I	30.56 N-14, II	21.6 N-14, III
		> -	122.24 N-18, IV	86.4 N-18, V	61.12 N-18, VI	43.2 N-14, IV	30.56 N-14, V	21.6 N-14, VI
	$\ell/\phi = 1$	> +				43.2 N-15, I	30.56 N-15, II	21.6 N-15, III
		> -				43.2 N-15, IV	30.56 N-15, V	21.6 N-15, VI

TABLE 4

EXPERIMENTS OF SYSTEMATIC STUDY

Variation of efficiency and voltage drop across the arc with the independent variables

1. Optimum choice of variables for best η, V_{arc}, $\overline{T}_g$

   (a) Polarities: For best η, V_{arc}, $\overline{T}_g$, > + has to be preferred to > -

   (b) Whatever the polarity:

For best	One must take					
	Polarity	$\mathcal{M}$	ℓ/ϕ	ϕ	m'	Injection Angle
η	> +	large	large	small	large	45°
	> -	large	small	unimportant at small m'; small at large m'	large	45°
V_{arc}	> +	large	large	small	large	45°
	> -	large	small	unimportant at small m'; small at large m'		45°
$\overline{T}_g$	Since $\overline{T}_g$ increases with $\frac{\eta P_{input}}{m'}$, i.e., increases with decreasing ϕ and decreasing mass flow, the "mass factor" $\mathcal{M}$, ratio of two small quantities, takes an "intermediate" value for optimum $\overline{T}_g$. The maximum temperatures ($\approx 10,000^{\circ}K$) were obtained for $\mathcal{M}$ = 20 to 30 (gr/sec. inches^2)					

TABLE 4 (CONTINUED)

2. *Variation of Efficiency*

Fixed Quantities	Polarity Case	Variation of Efficiency	Independent Variable
power input, geometry, mass flow	--	$\eta_{>+} > \eta_{>-}$	polarity
polarity, geometry, mass flow	all	$\eta \searrow$	$P_{input} \nearrow$
polarity, mass flow, power input and ϕ fixed, ℓ/ϕ variable	> +	$\eta \nearrow$	$\ell/\phi \nearrow$
	> -	$\eta \searrow$	$\ell/\phi \nearrow$
ℓ/ϕ fixed, ϕ variable	> +	$\eta \searrow$	$\phi \nearrow$
	> -	small mass flows: practically unaffected	$\phi \nearrow$
		large mass flows: $\eta \searrow$	$\phi \nearrow$
polarity, geometry, power input	all	$\eta \nearrow$	m' $\nearrow$
polarity, ℓ/ϕ, power input	all	$\eta \nearrow$	$\mathcal{H} \nearrow$

TABLE 4 (CONTINUED)

3. Variation of Voltage Drop Across the Arc			
Fixed Quantities	Polarity Case	Variation of V_{arc}	Independent Variable
polarity, geometry, mass flow	> +	V_{arc} ↗	P_{input} ↗
polarity, geometry, power input	all	V_{arc} ↗	m' ↗
polarity, mass flow, current			
∅ fixed, $\ell/\emptyset$ variable	> +	V_{arc} ↗	$\ell/\emptyset$ ↗
	> -	V_{arc} ≈ constant	$\ell/\emptyset$ ↗
$\ell/\emptyset$ fixed, ∅ variable	> +	V_{arc} ↘	∅ ↗
	> -	V_{arc} ↗ slightly at small mass flow	∅ ↗
		V_{arc} ↘ at large mass flow	
polarity, $\ell/\emptyset$, current		V_{arc} ↗ (strongly)	ℋ ↗

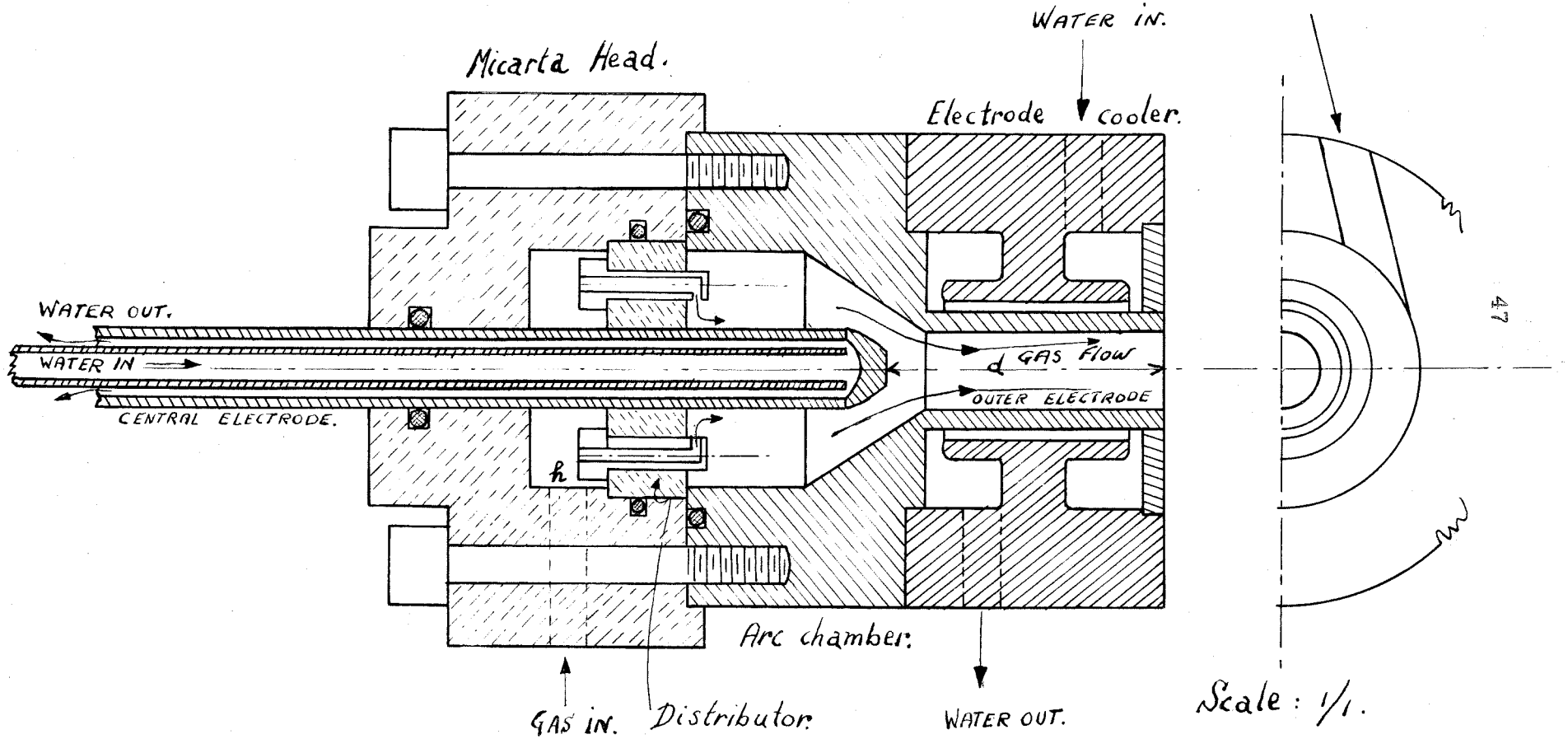

Fig. 1 Arc heater.

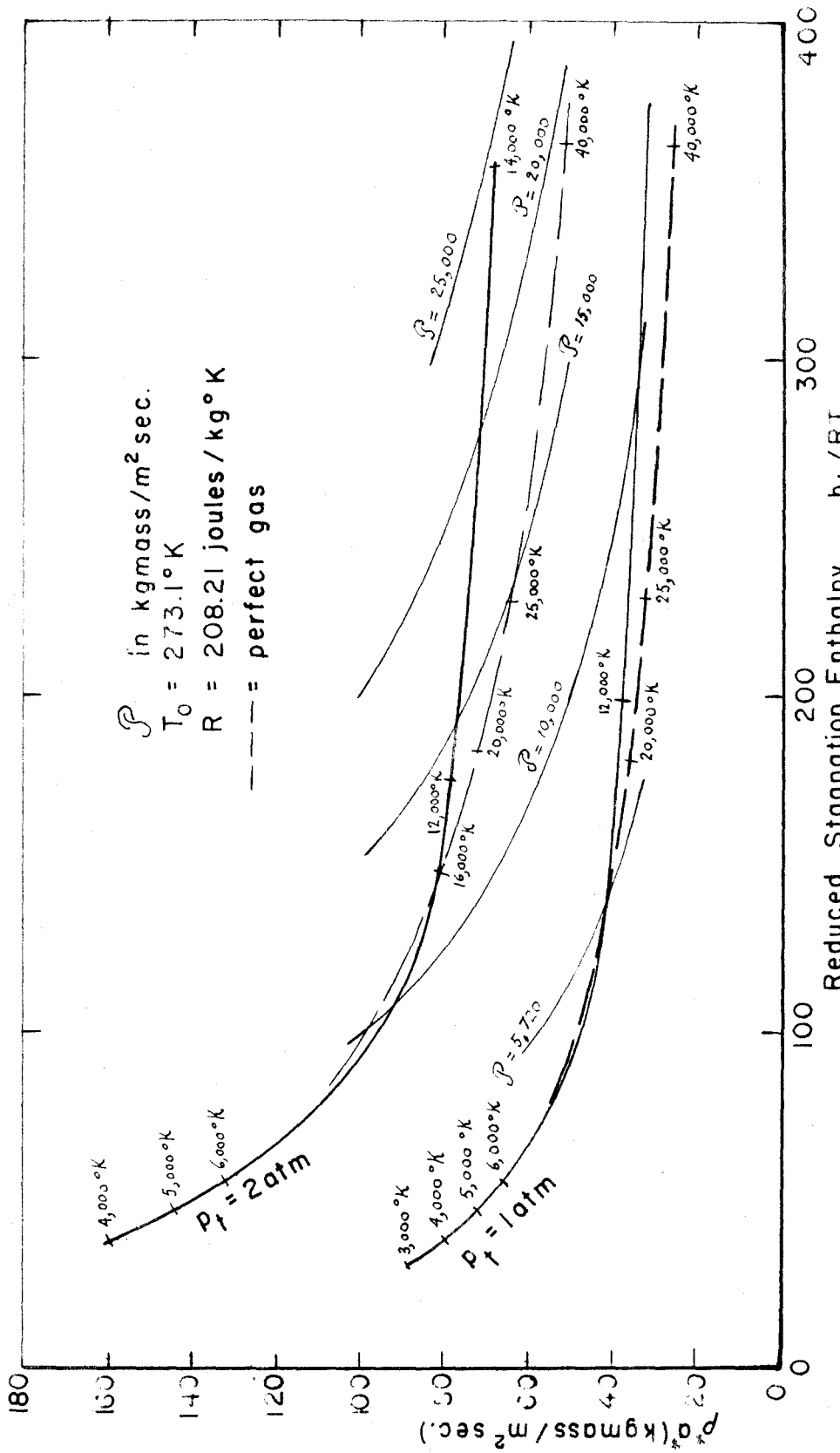

FIG. 2 CURVES $\rho^* a^* = \mathcal{P}\left(\frac{ht}{RT_0}\right)$ and $\mathcal{P}$ = CONSTANT

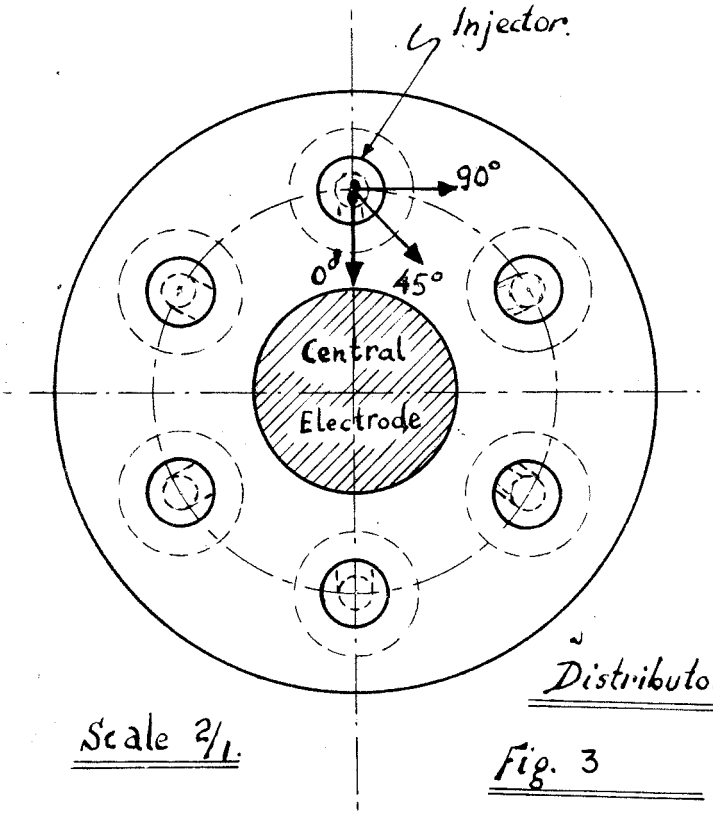

Distributor.

Scale 2/1.

Fig. 3

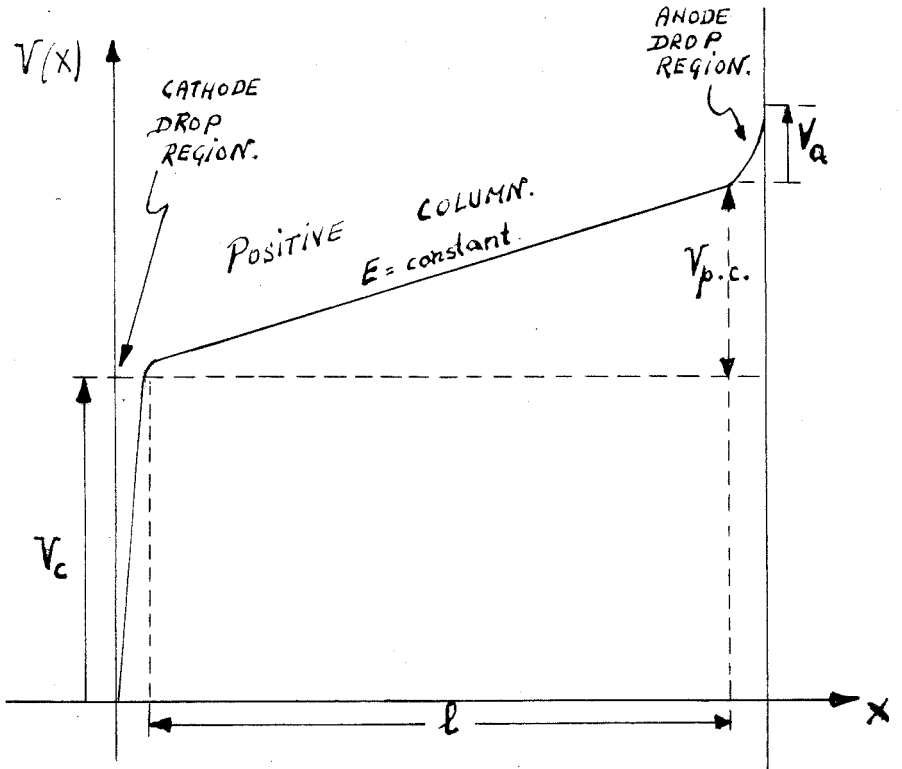

Potential - distribution
Static case.

Fig. 4

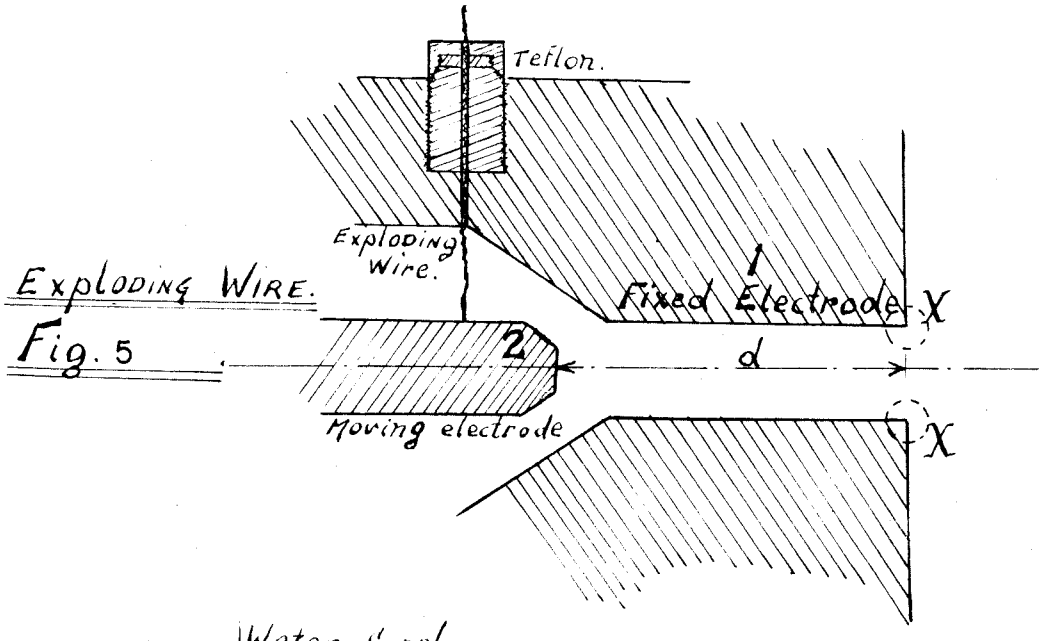

Exploding Wire.

Fig. 5

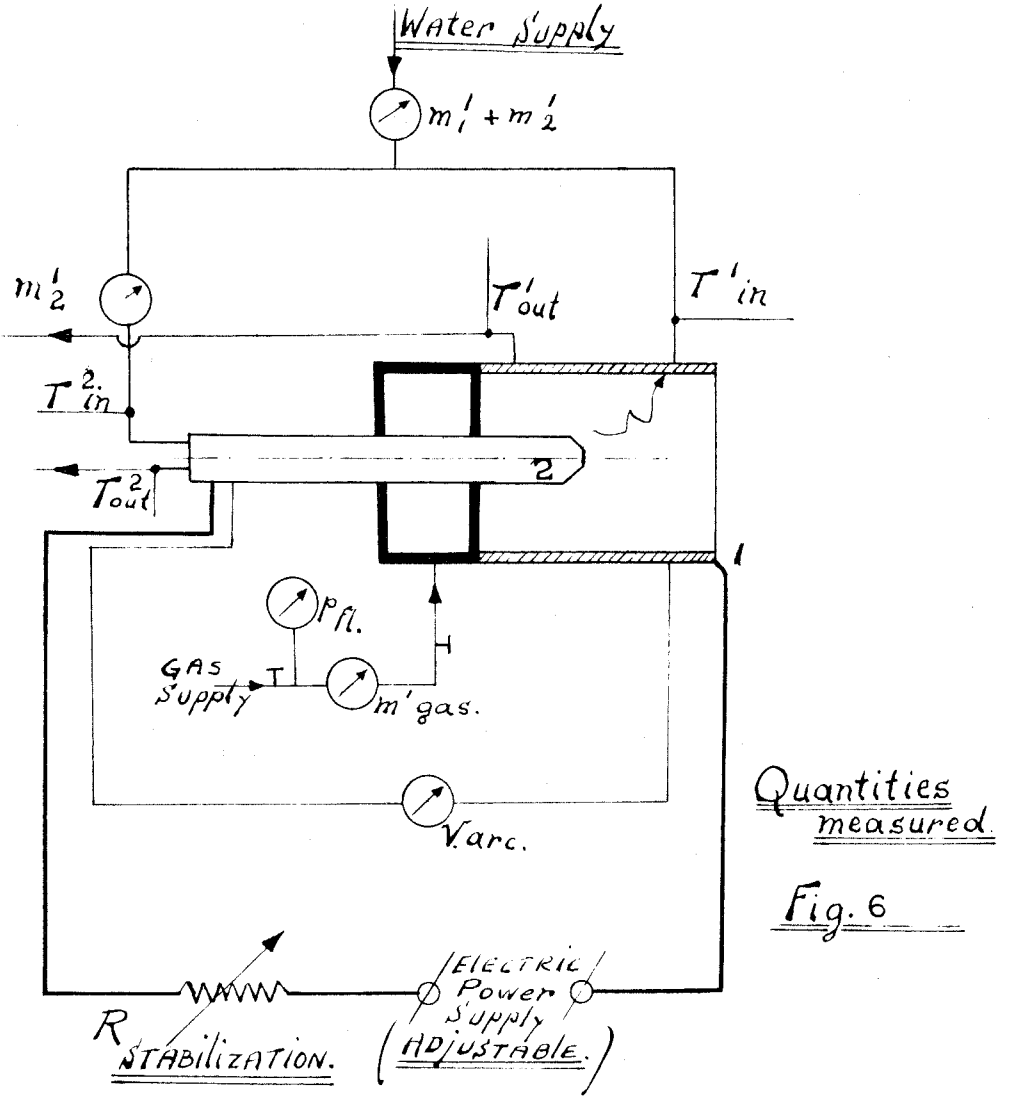

Quantities measured

Fig. 6

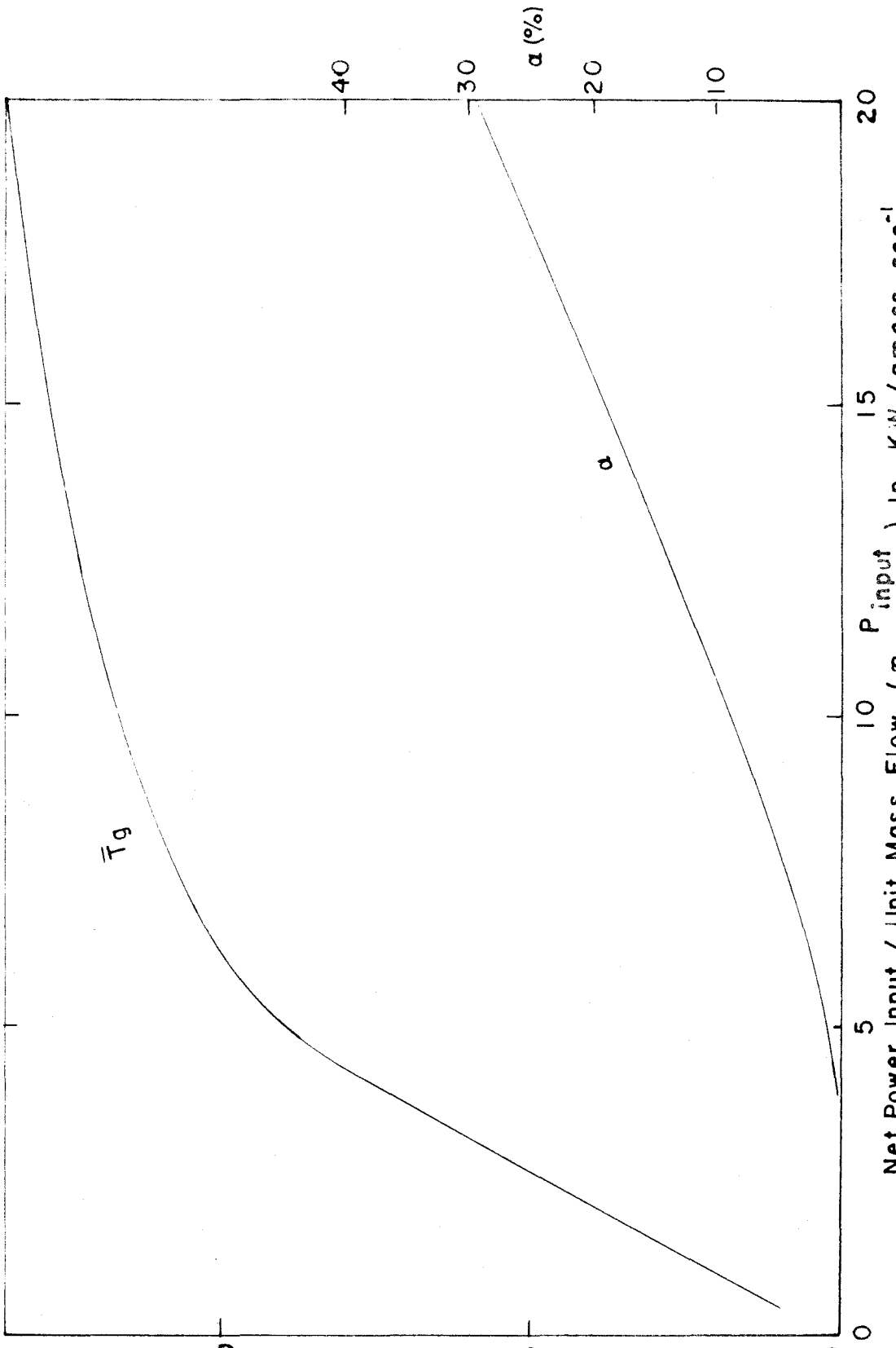

FIG. 7 ARGON AT P = 1 ATM.

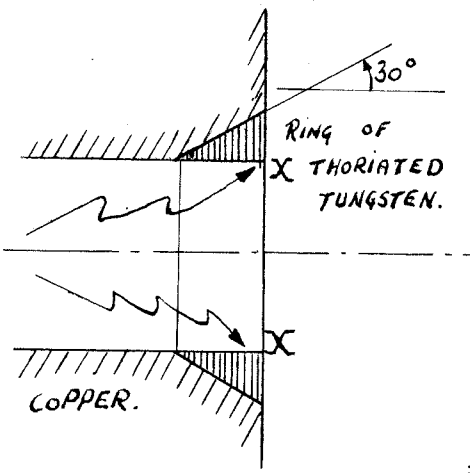

Fig. 8

Sharp edge XX.

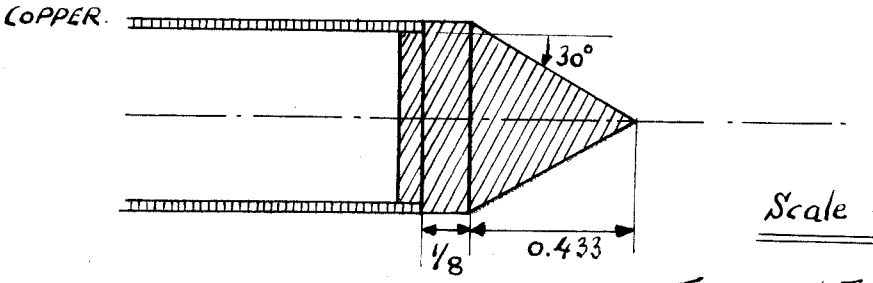

Scale 2/1.

Thoriated Tungsten tip.

Fig. 9

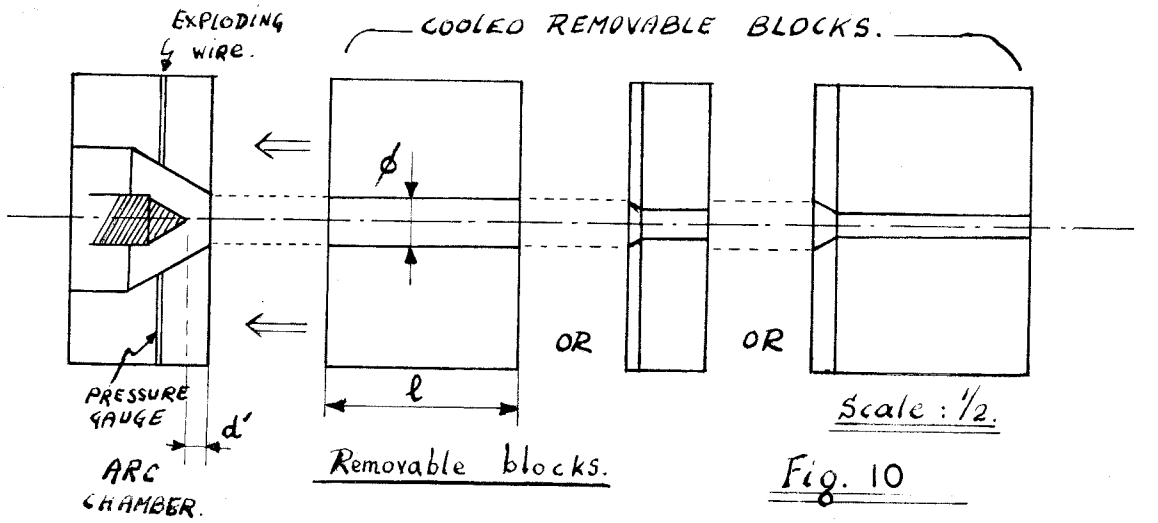

Fig. 10

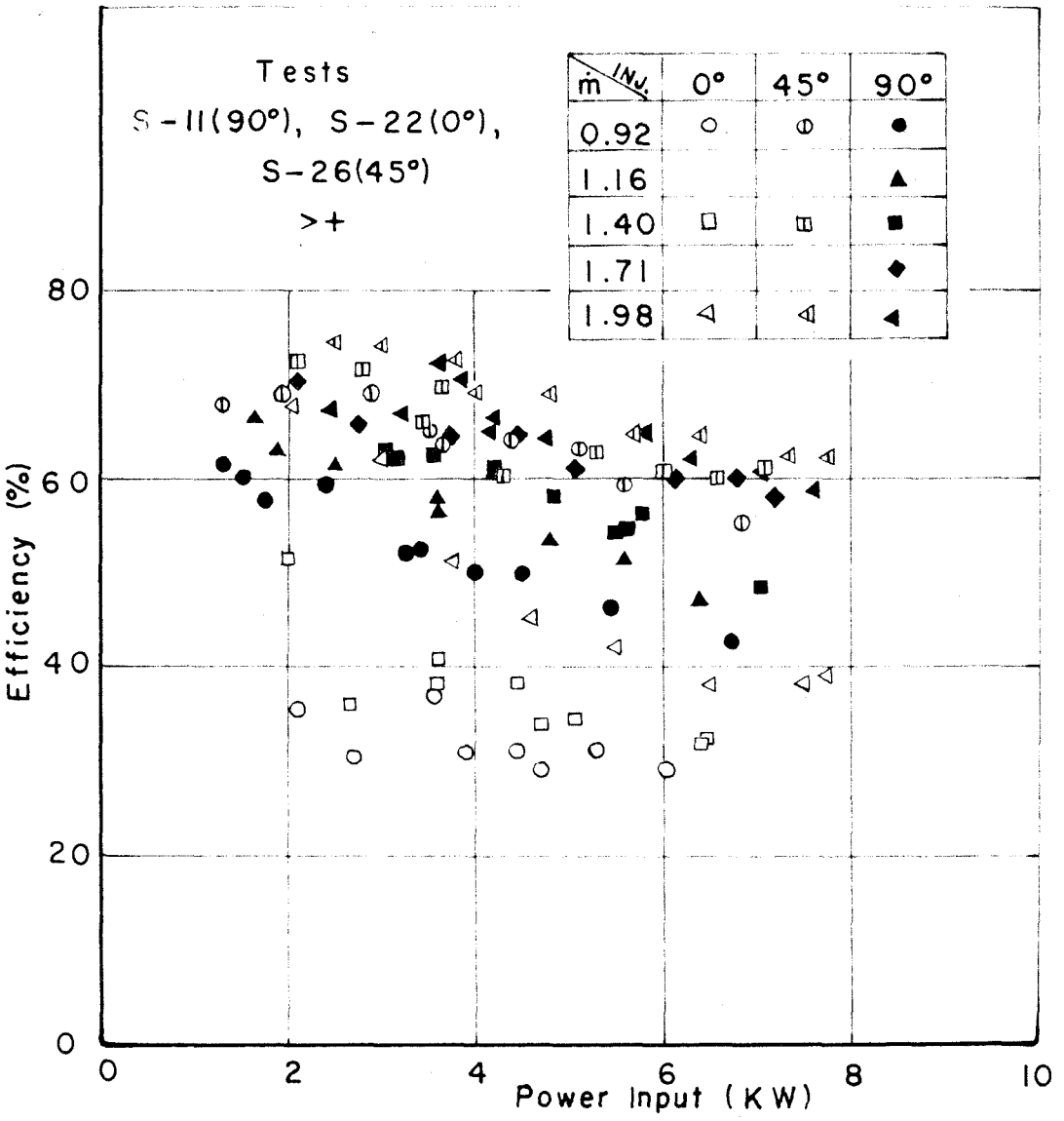

FIG. 11 EFFICIENCY η VS. GROSS POWER INPUT

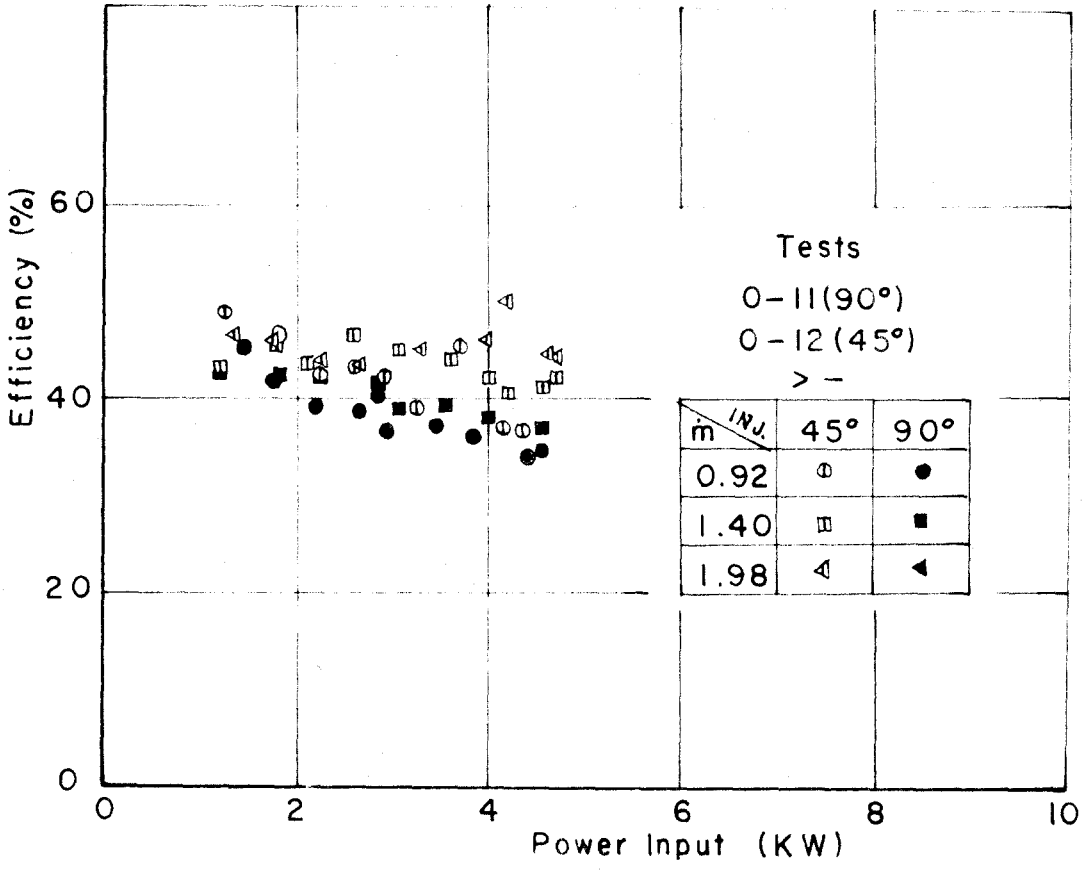

FIG. 12 EFFICIENCY η VS. GROSS POWER INPUT

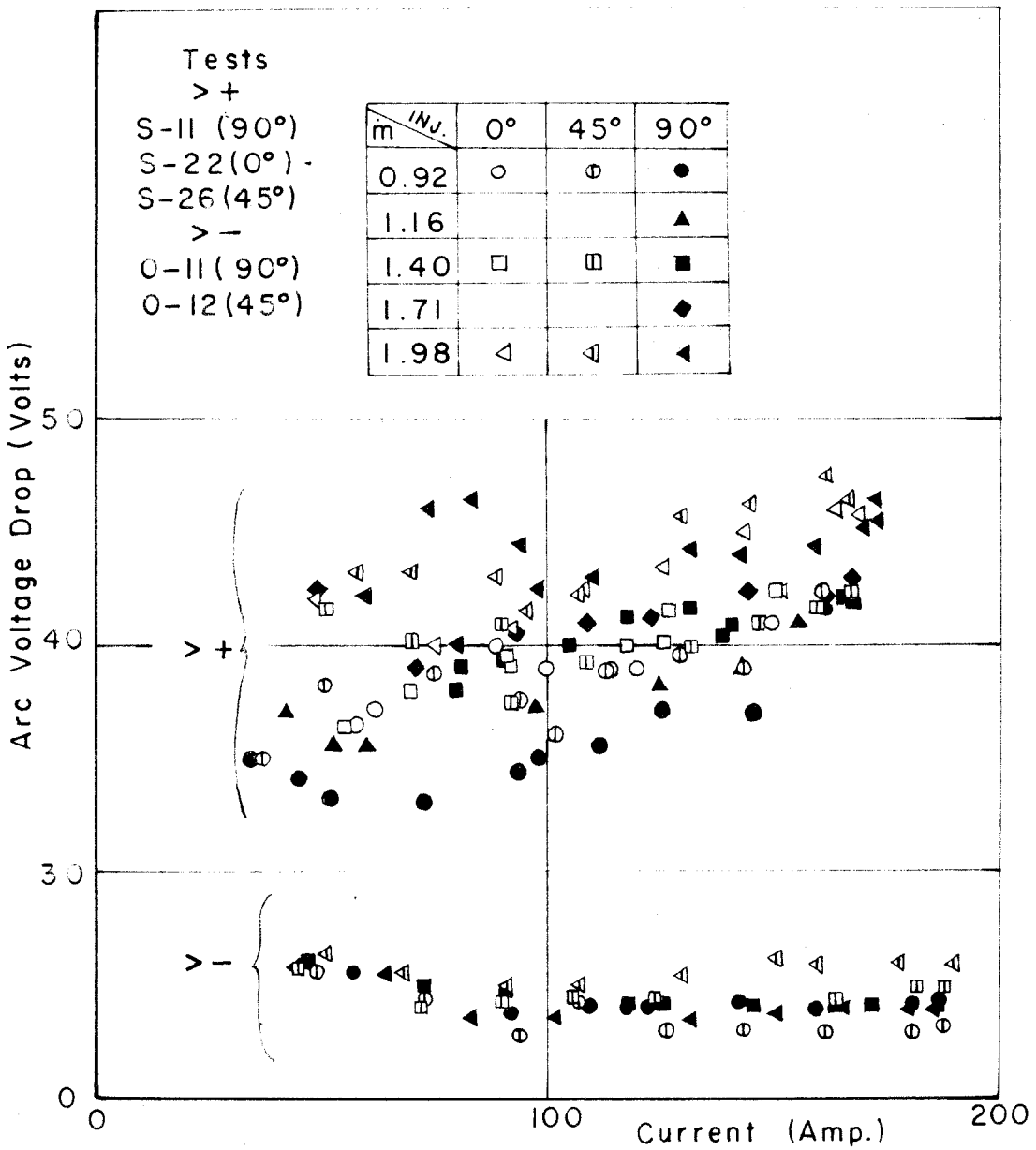

FIG. 13 ARC VOLTAGE DROP VS. CURRENT

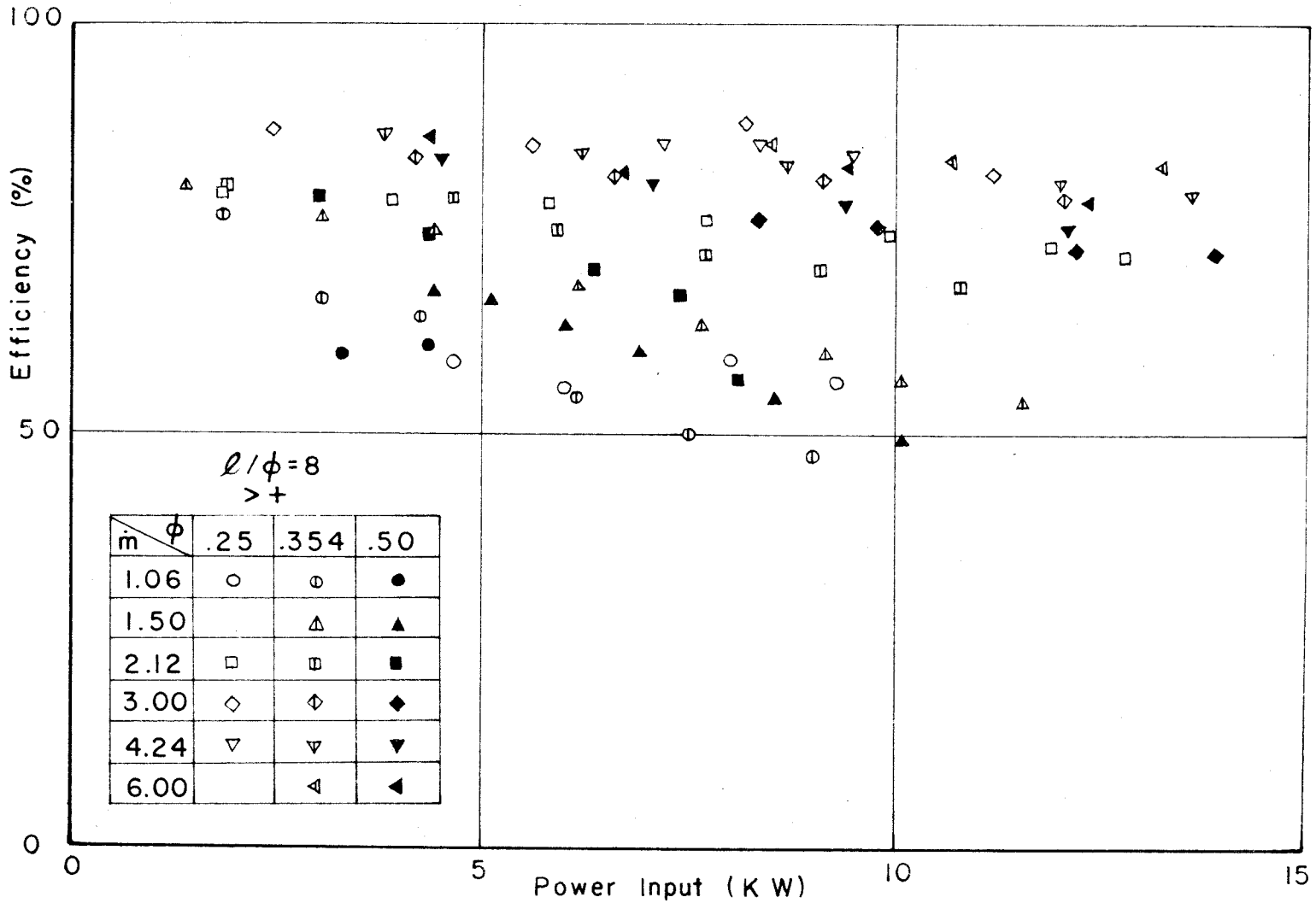

FIG. 14 EFFICIENCY η VS. GROSS POWER INPUT

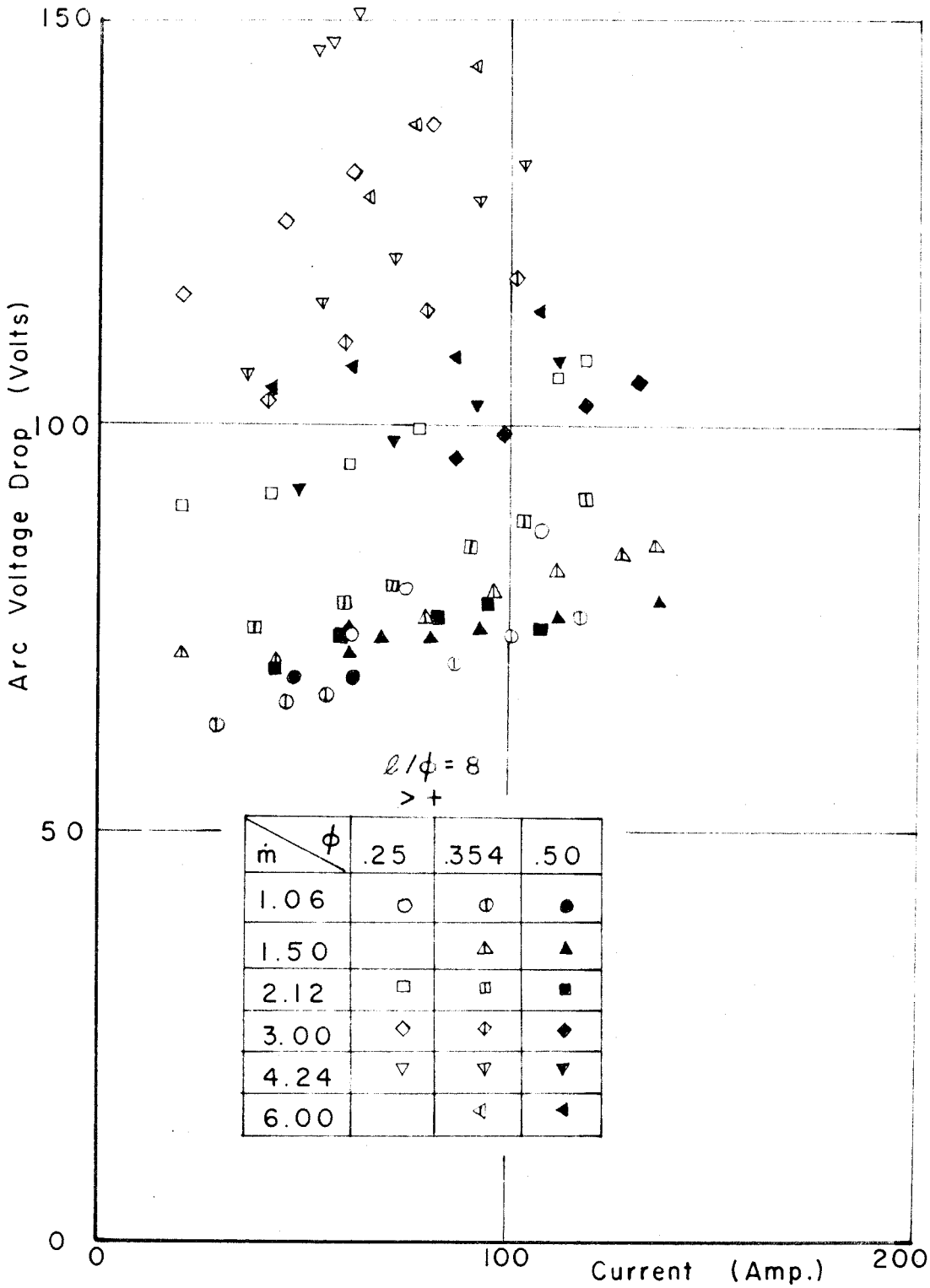

FIG. 15 ARC VOLTAGE DROP VS. CURRENT

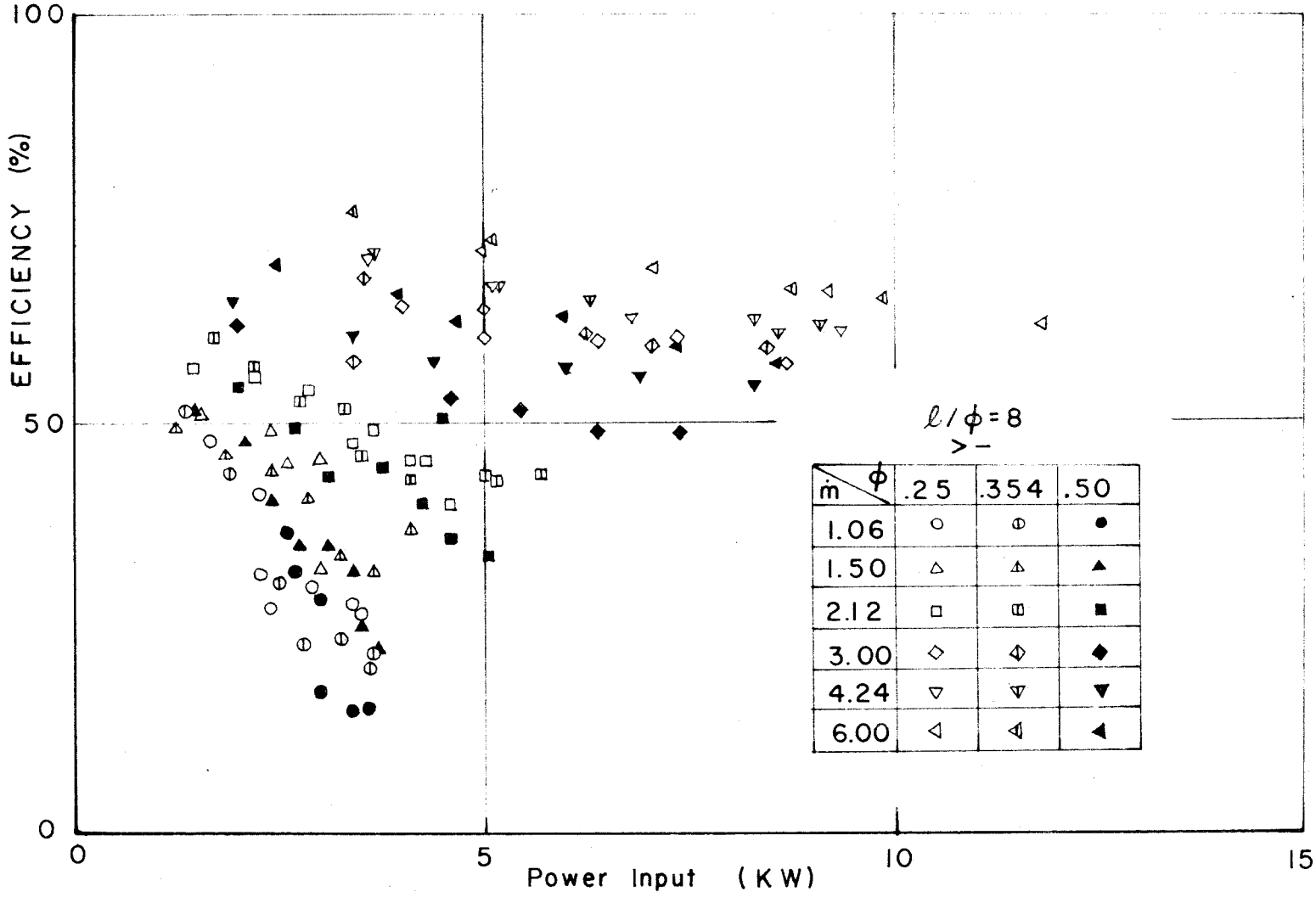

FIG. 16 EFFICIENCY η VS. GROSS POWER INPUT

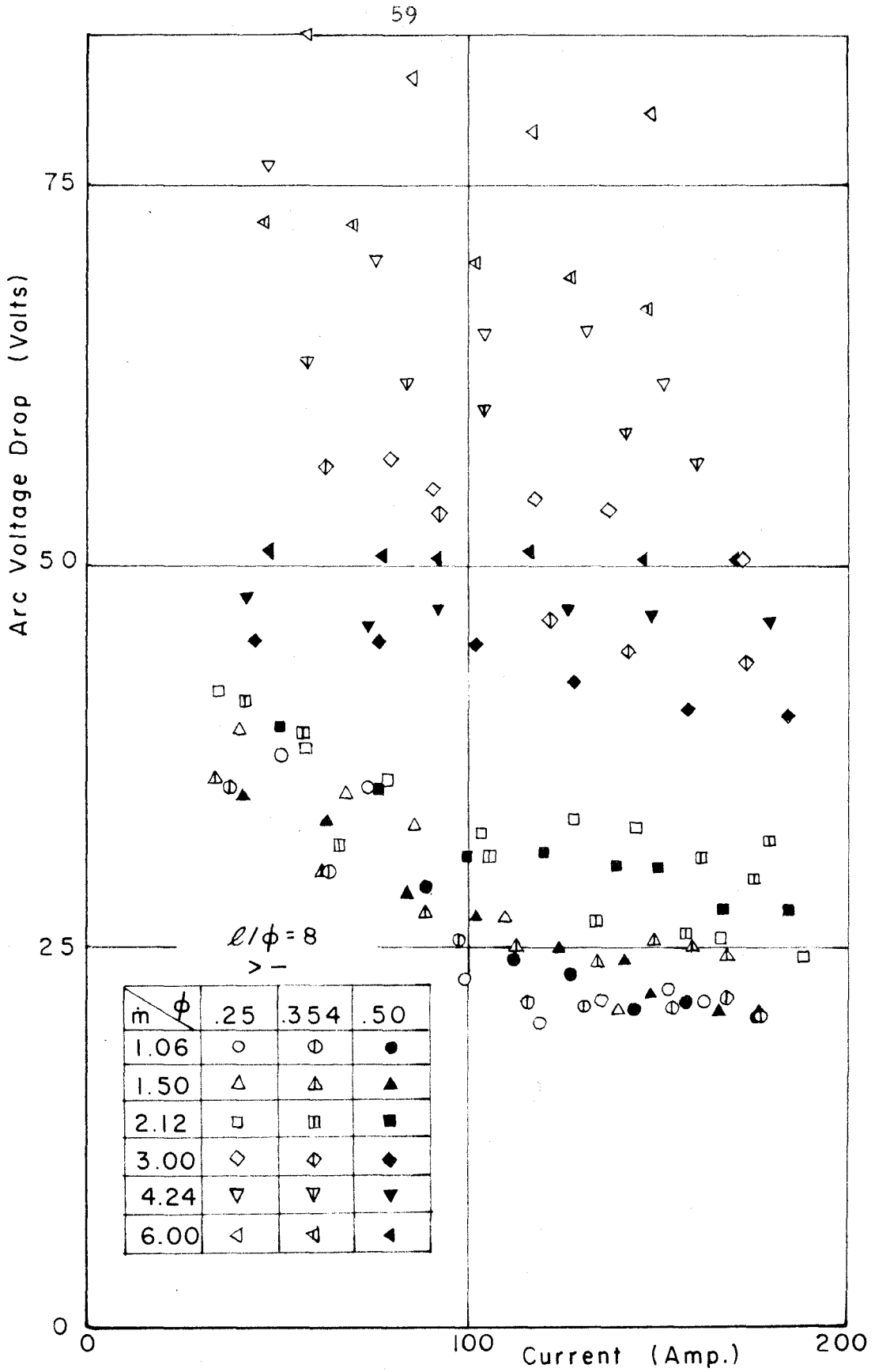

FIG. 17 ARC VOLTAGE DROP VS. CURRENT

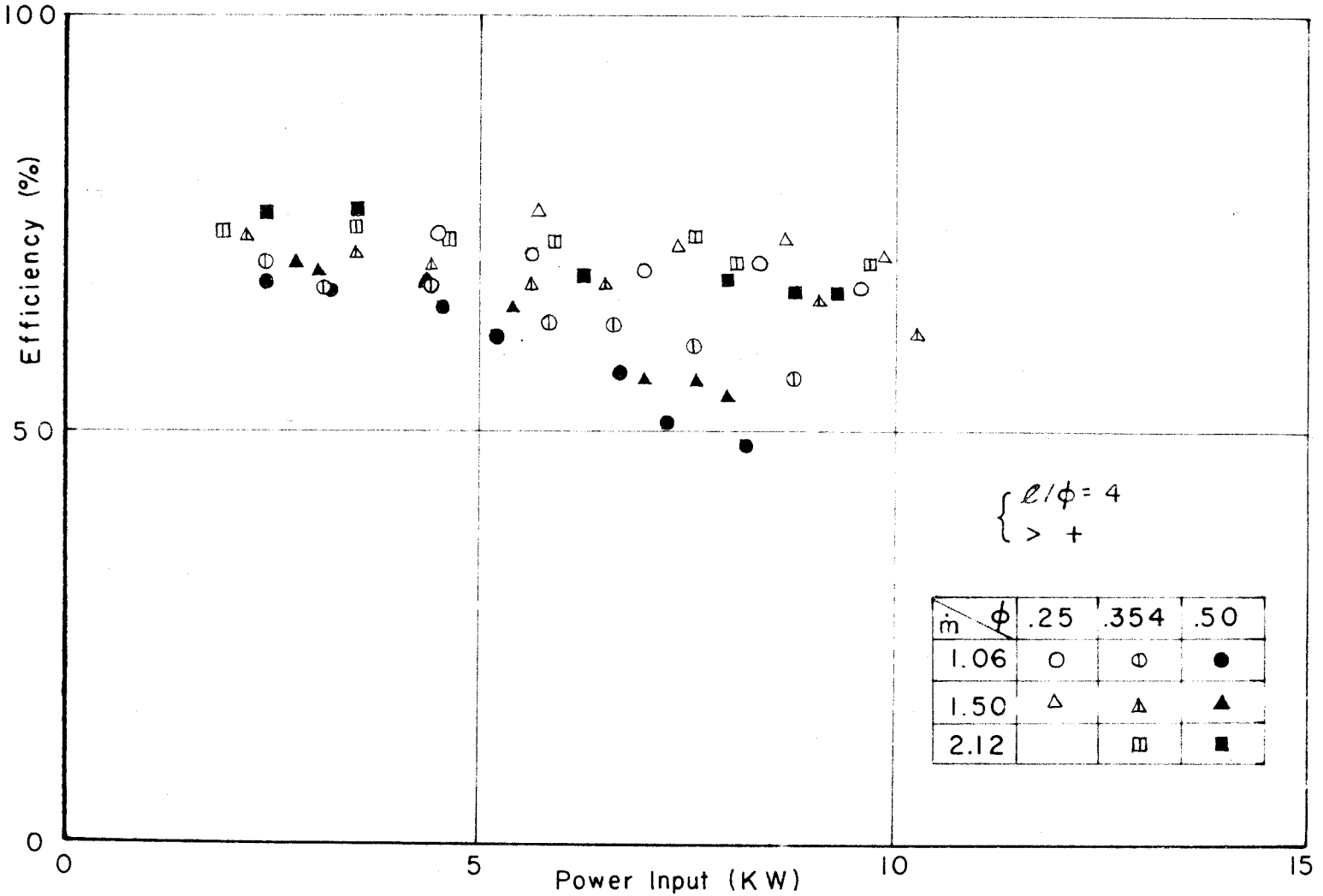

FIG. 18 EFFICIENCY η VS. GROSS POWER INPUT

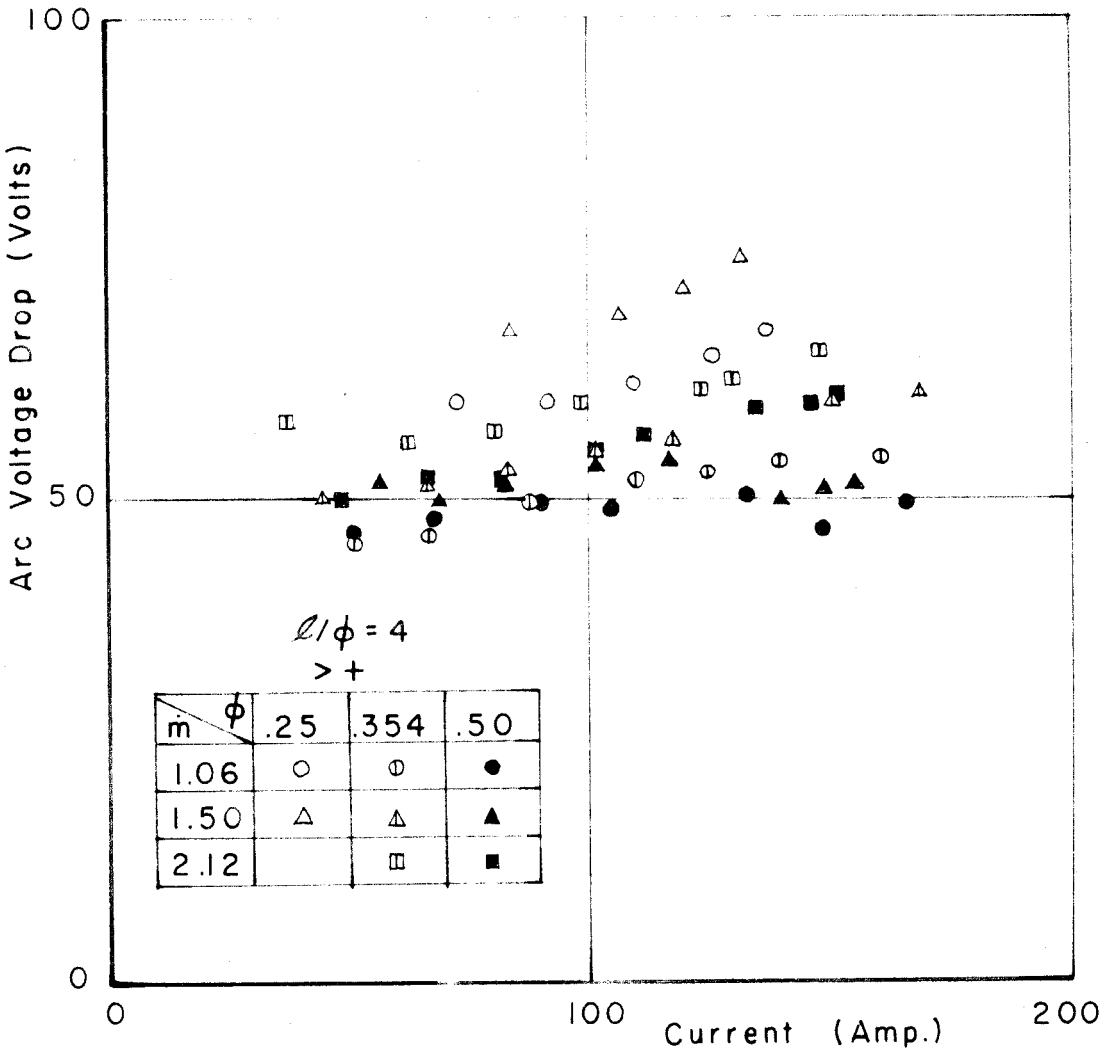

FIG. 19 ARC VOLTAGE DROP VS. CURRENT

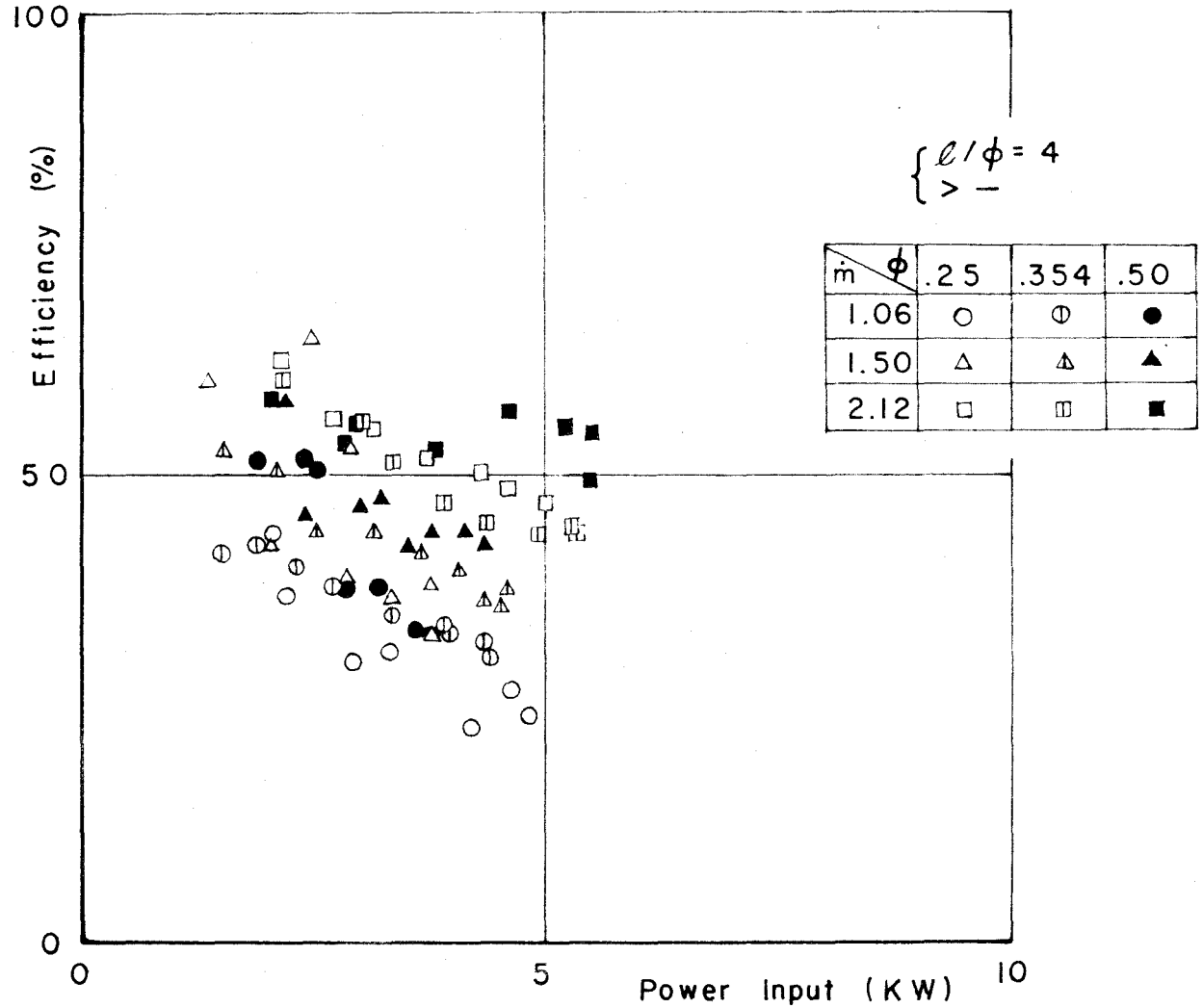

FIG. 20 EFFICIENCY VS. GROSS POWER INPUT

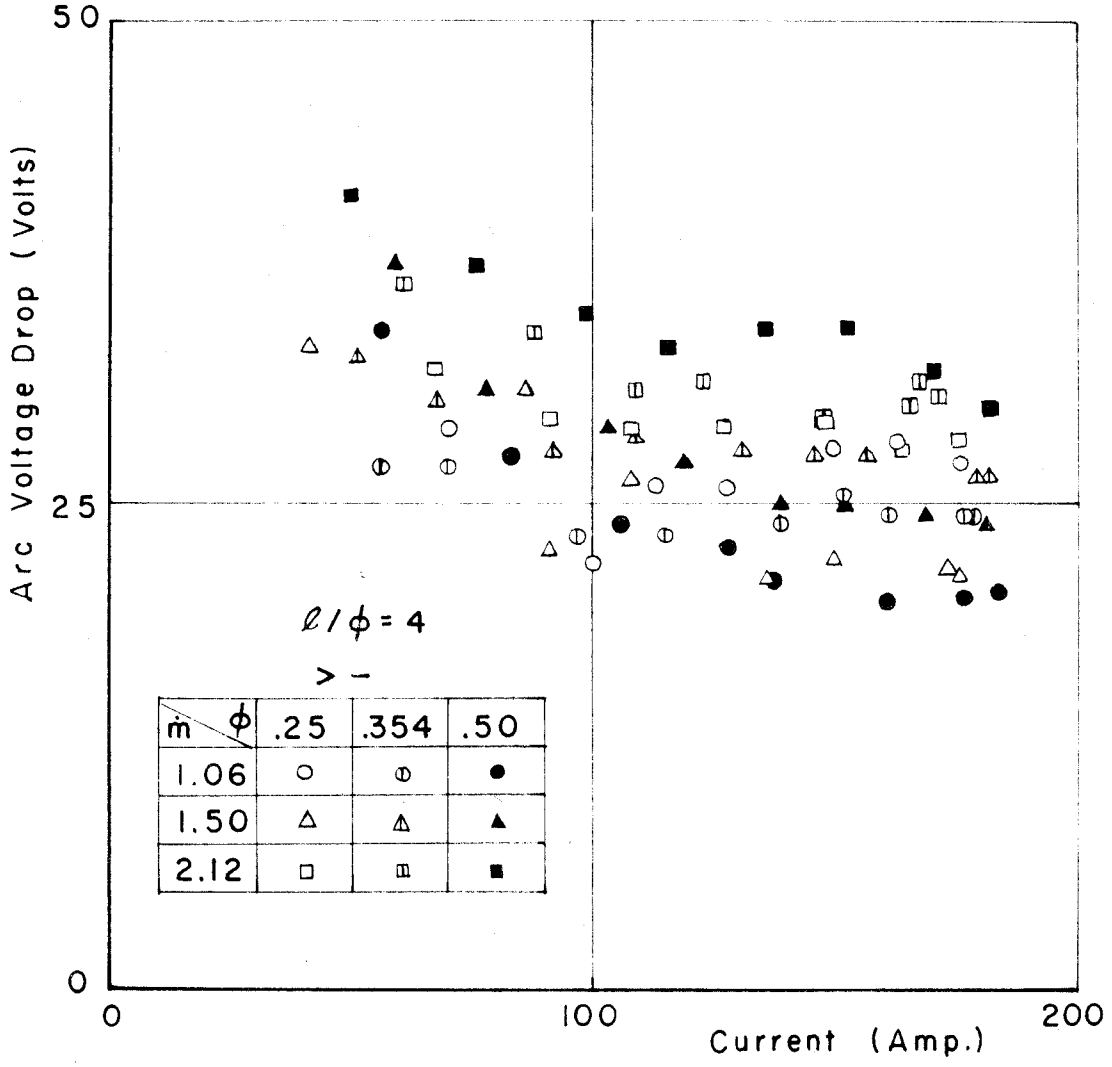

FIG. 21 ARC VOLTAGE DROP VS. CURRENT

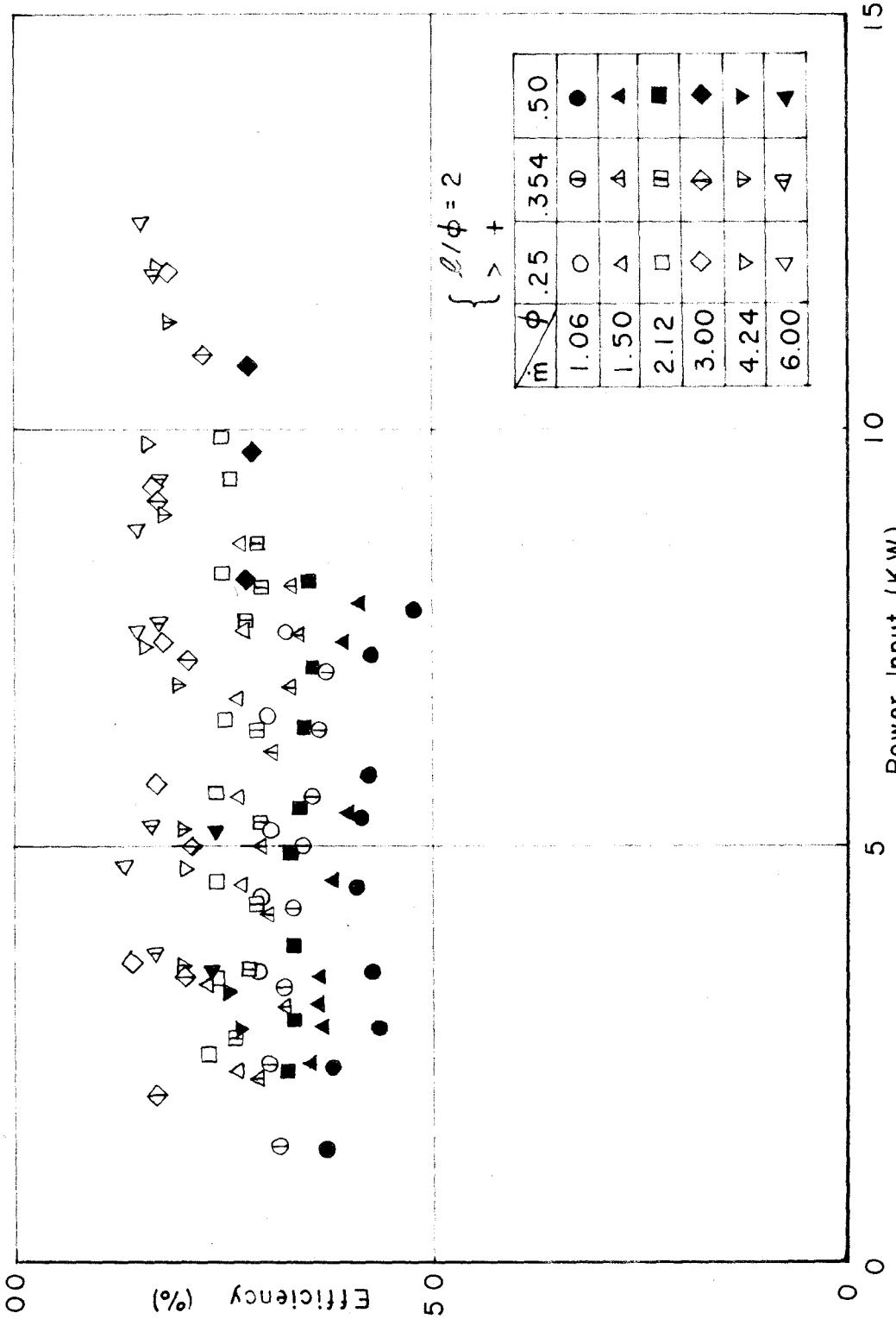

FIG. 22 EFFICIENCY η VS. GROSS POWER INPUT

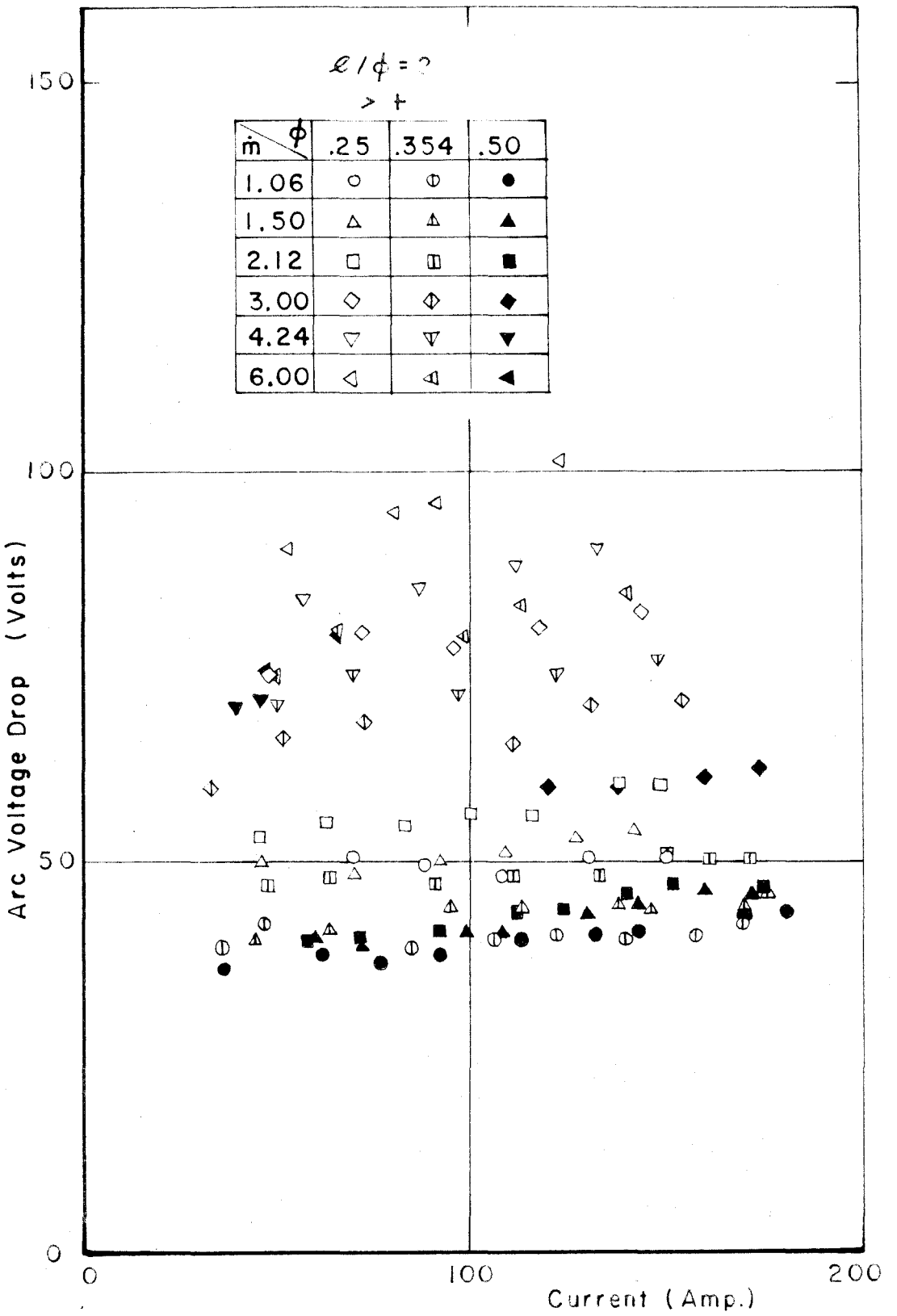

FIG. 23 ARC VOLTAGE DROP VS. CURRENT

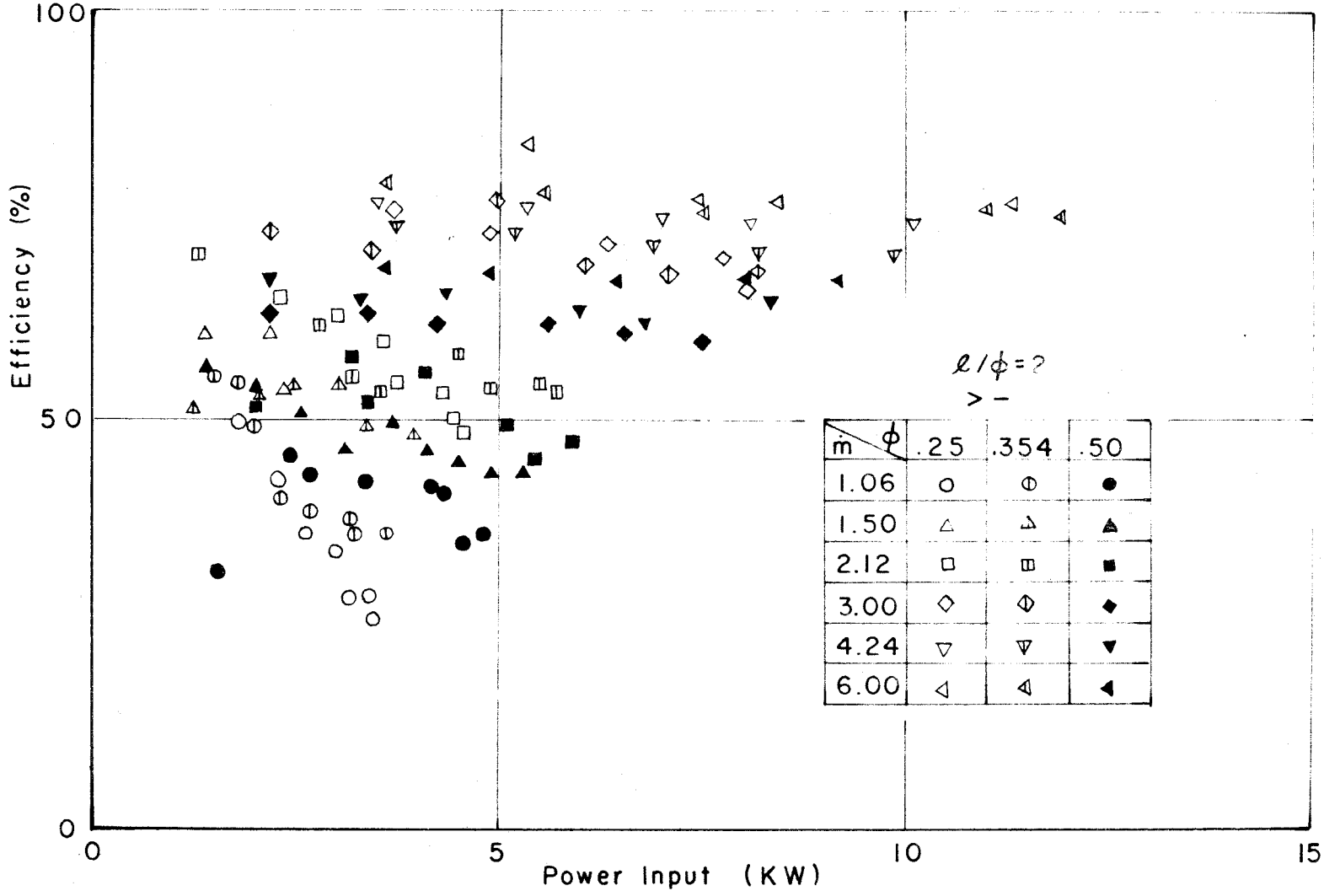

FIG. 24 EFFICIENCY η VS. GROSS POWER INPUT

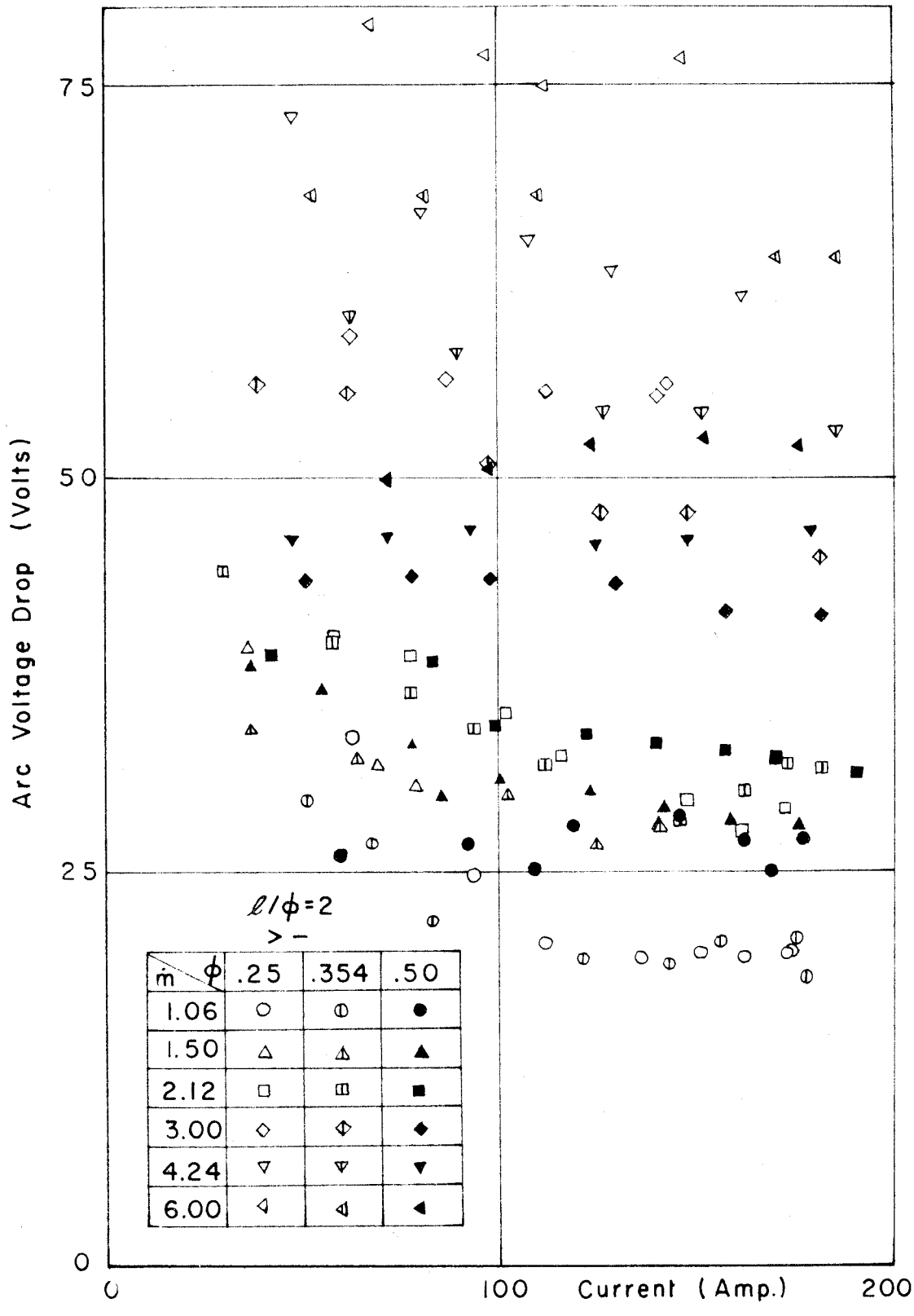

FIG. 25 ARC VOLTAGE DROP VS. CURRENT

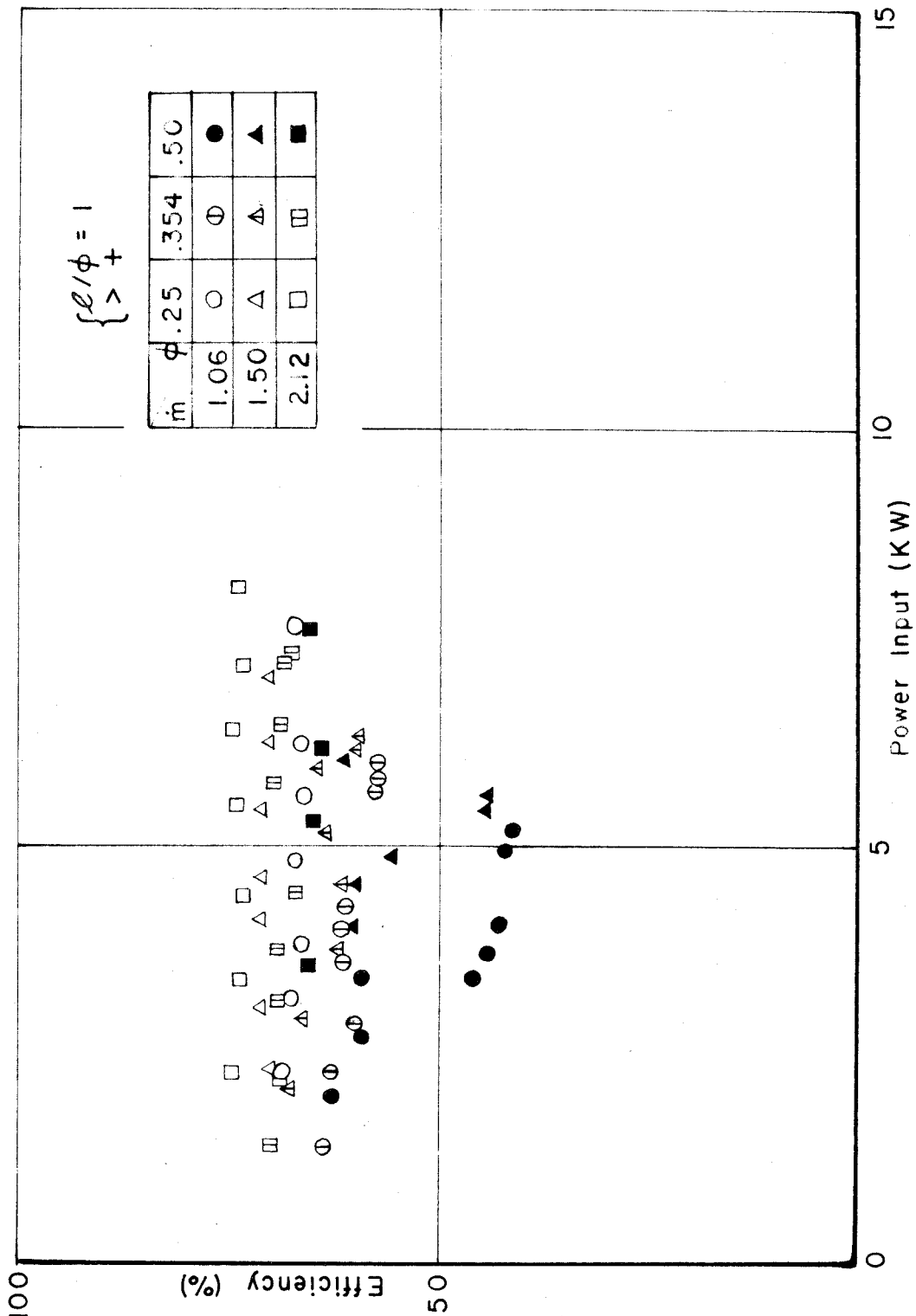

FIG. 26 EFFICIENCY η VS. GROSS POWER INPUT

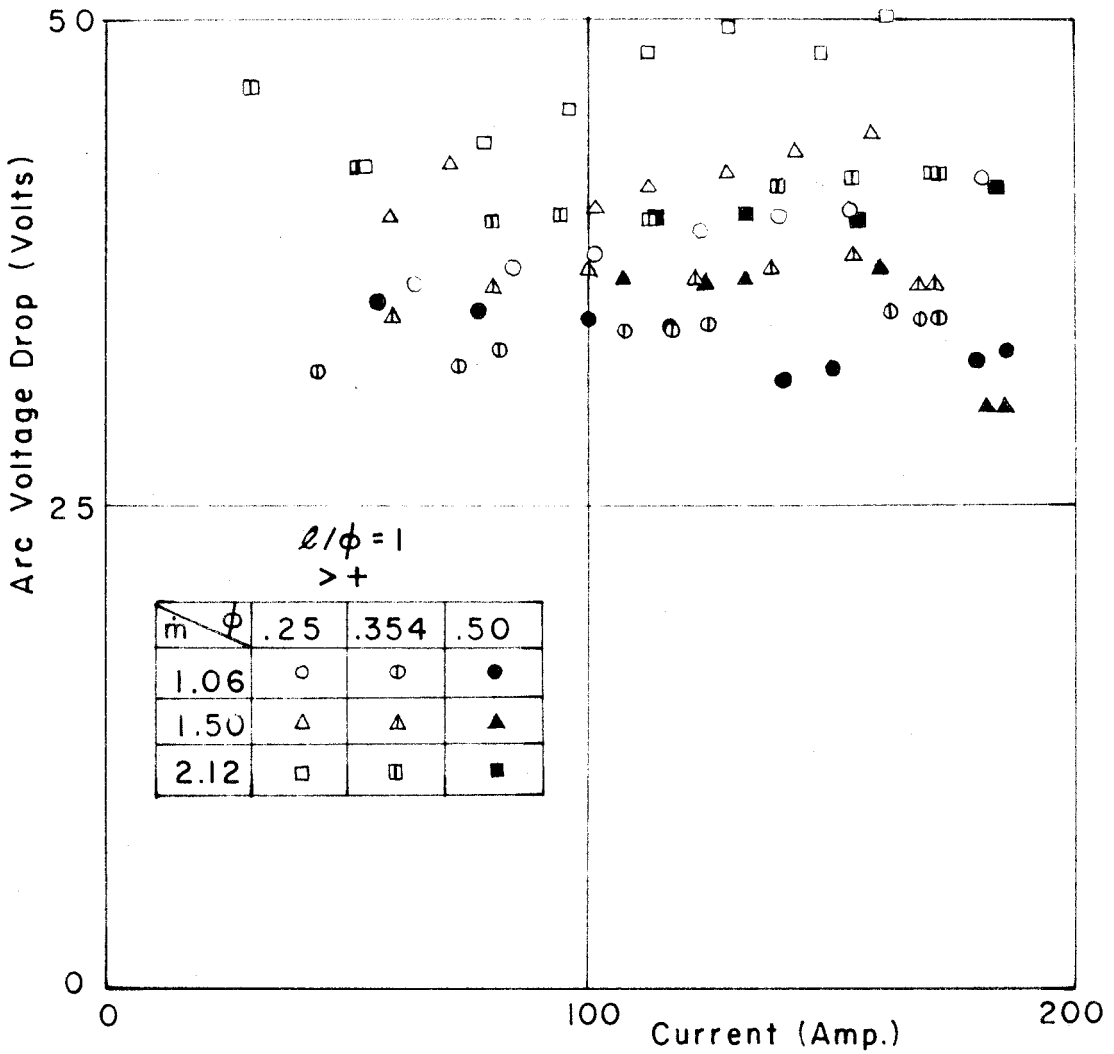

FIG. 27 ARC VOLTAGE DROP VS. CURRENT

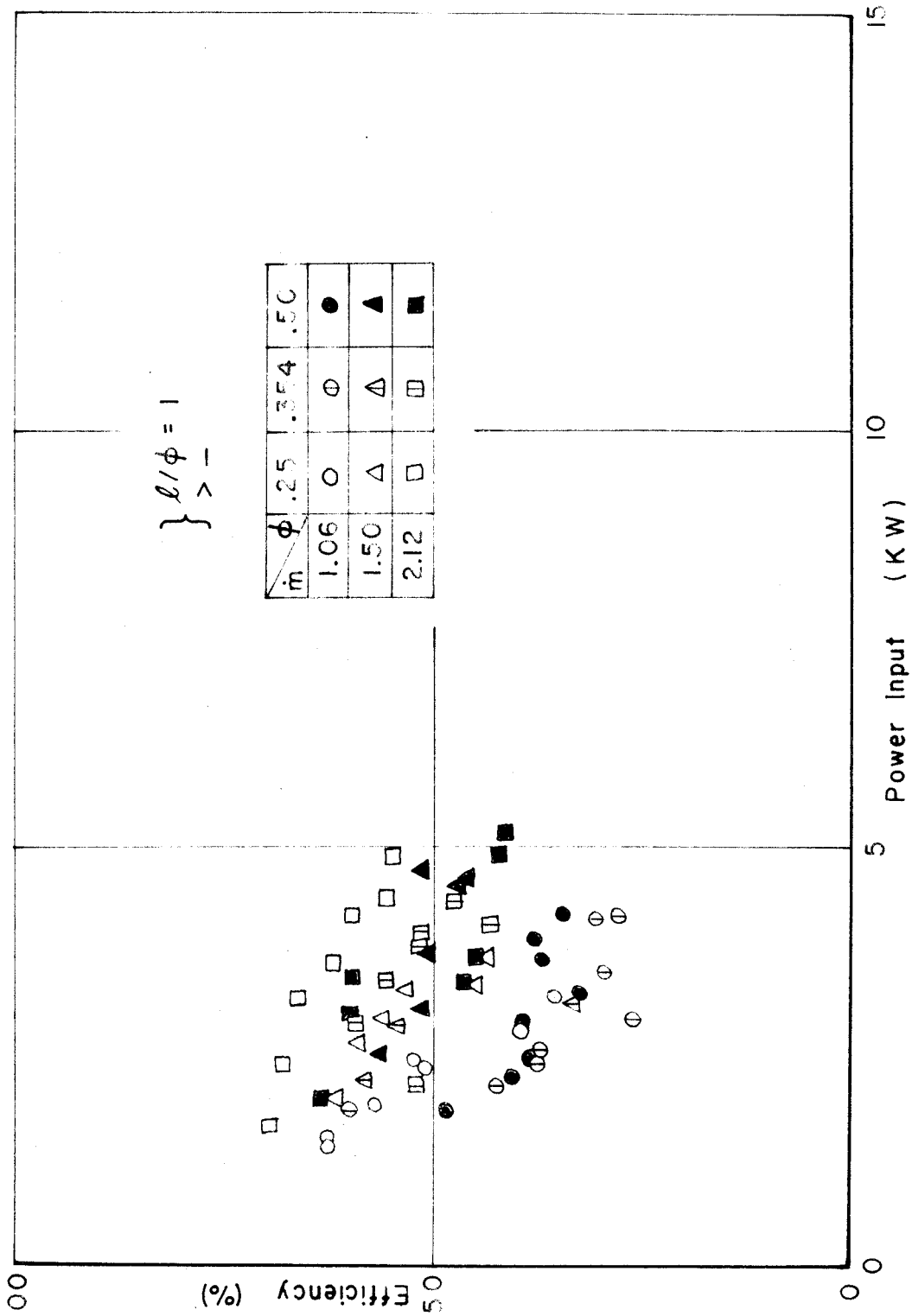

FIG. 28 EFFICIENCY η VS. GROSS POWER INPUT

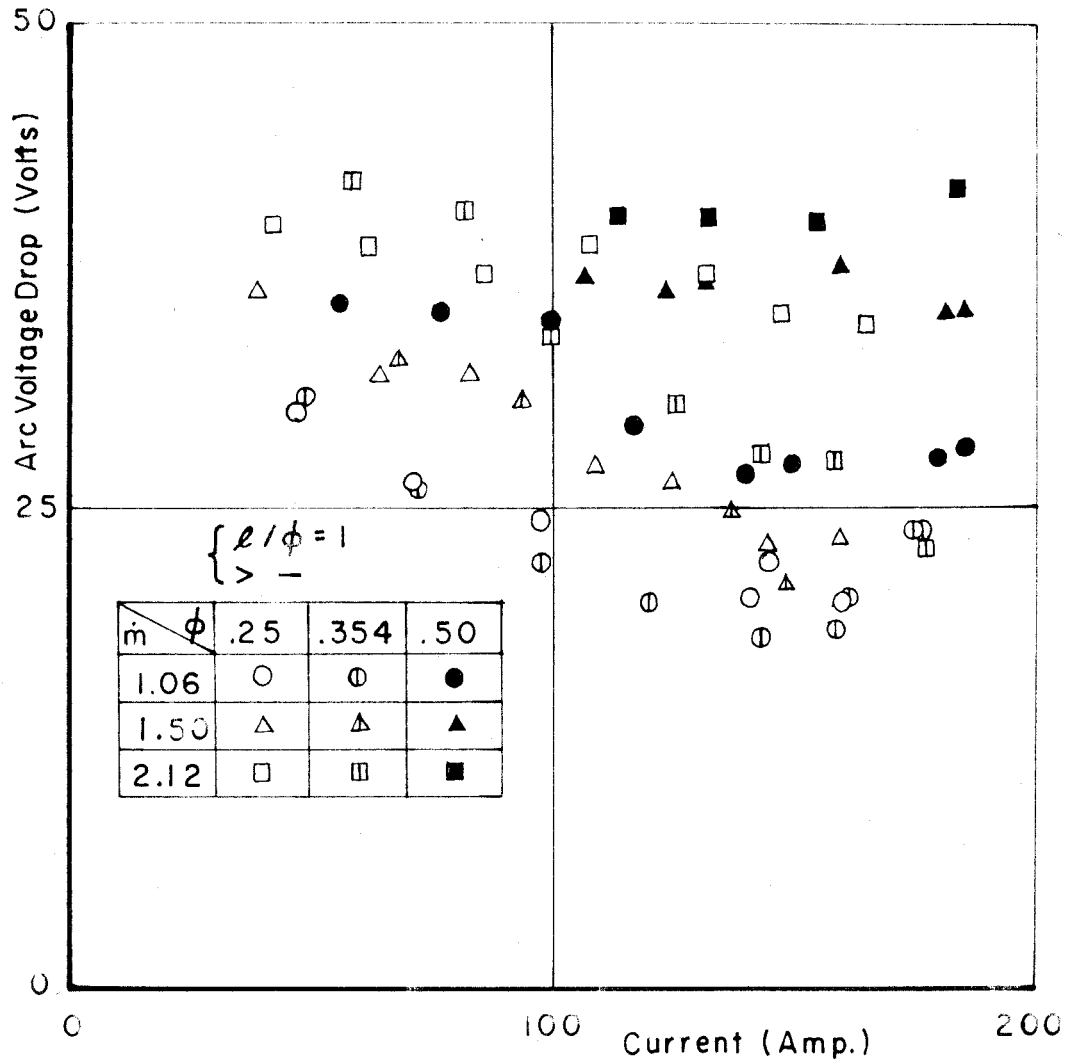

FIG. 29 ARC VOLTAGE DROP VS. CURRENT

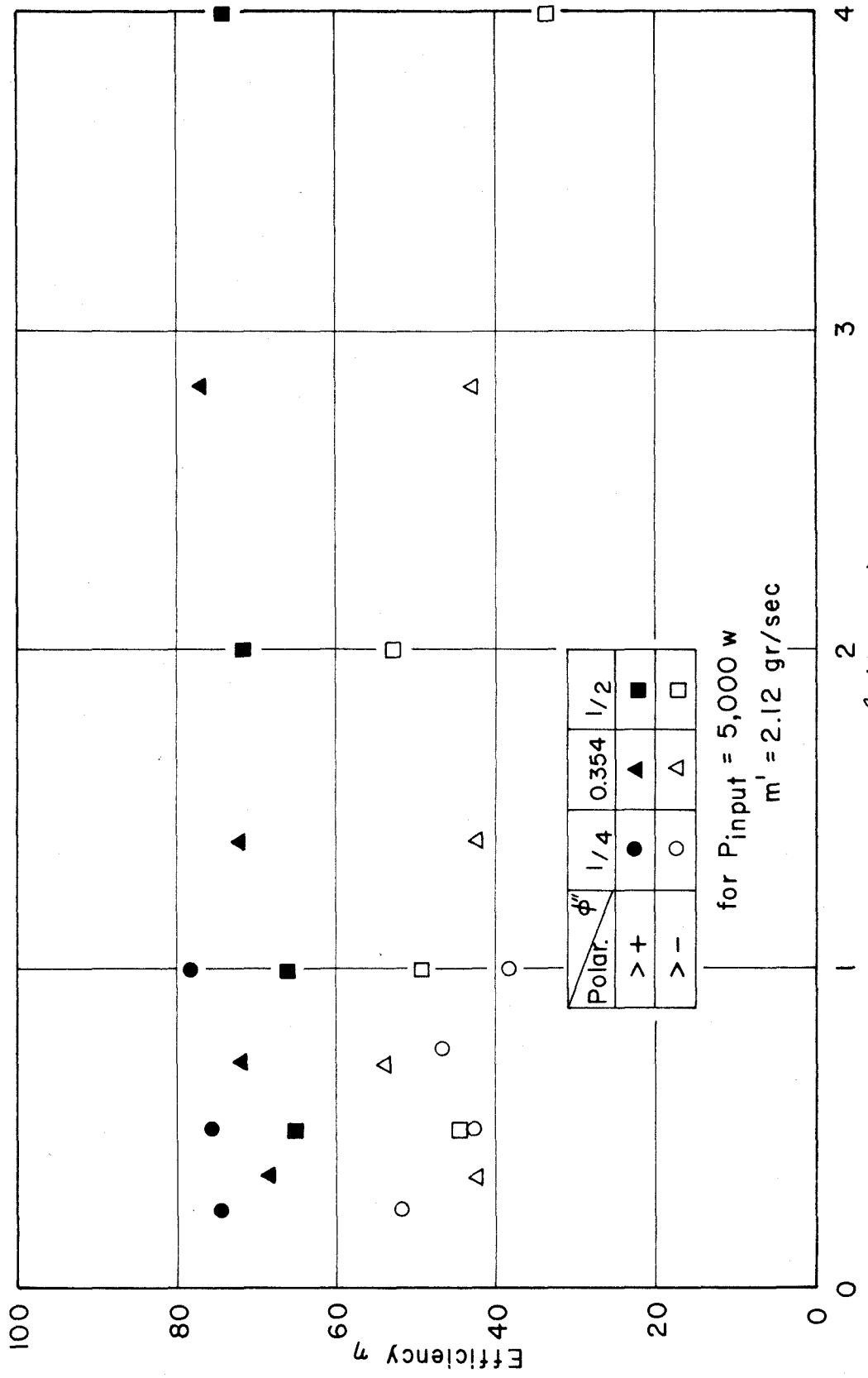

FIG. 30 EFFICIENCY VS. LENGTH ℓ OF CONSTRICTING CHANNEL

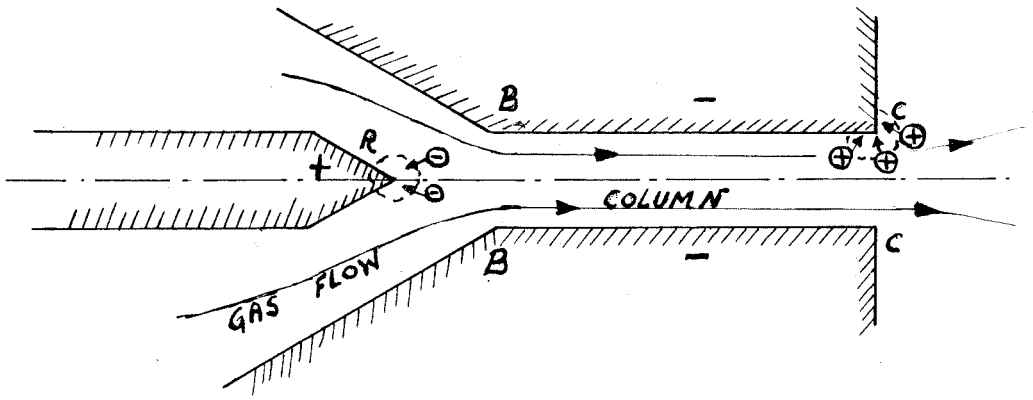

>+ Configuration.

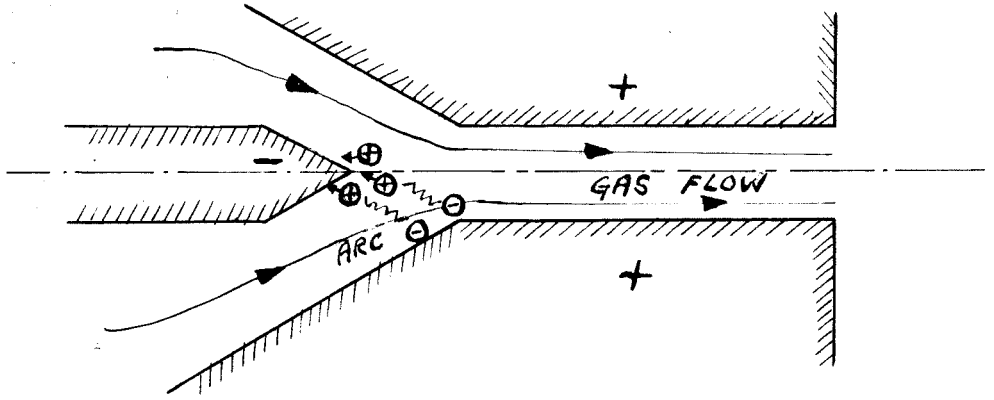

>– Configuration.

Fig. 31

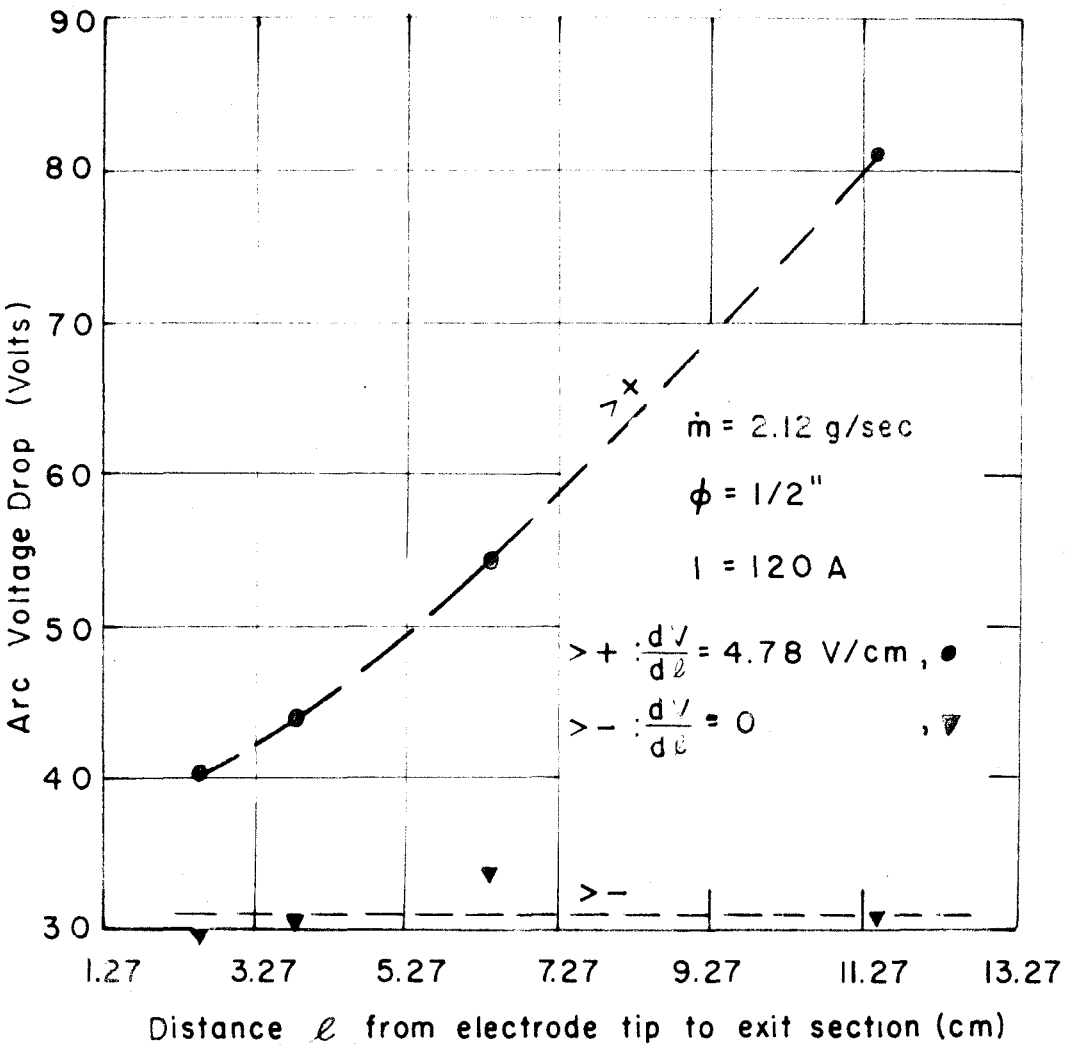

FIG. 32 ARC VOLTAGE DROP VS. DISTANCE TIP-EXIT SECTION

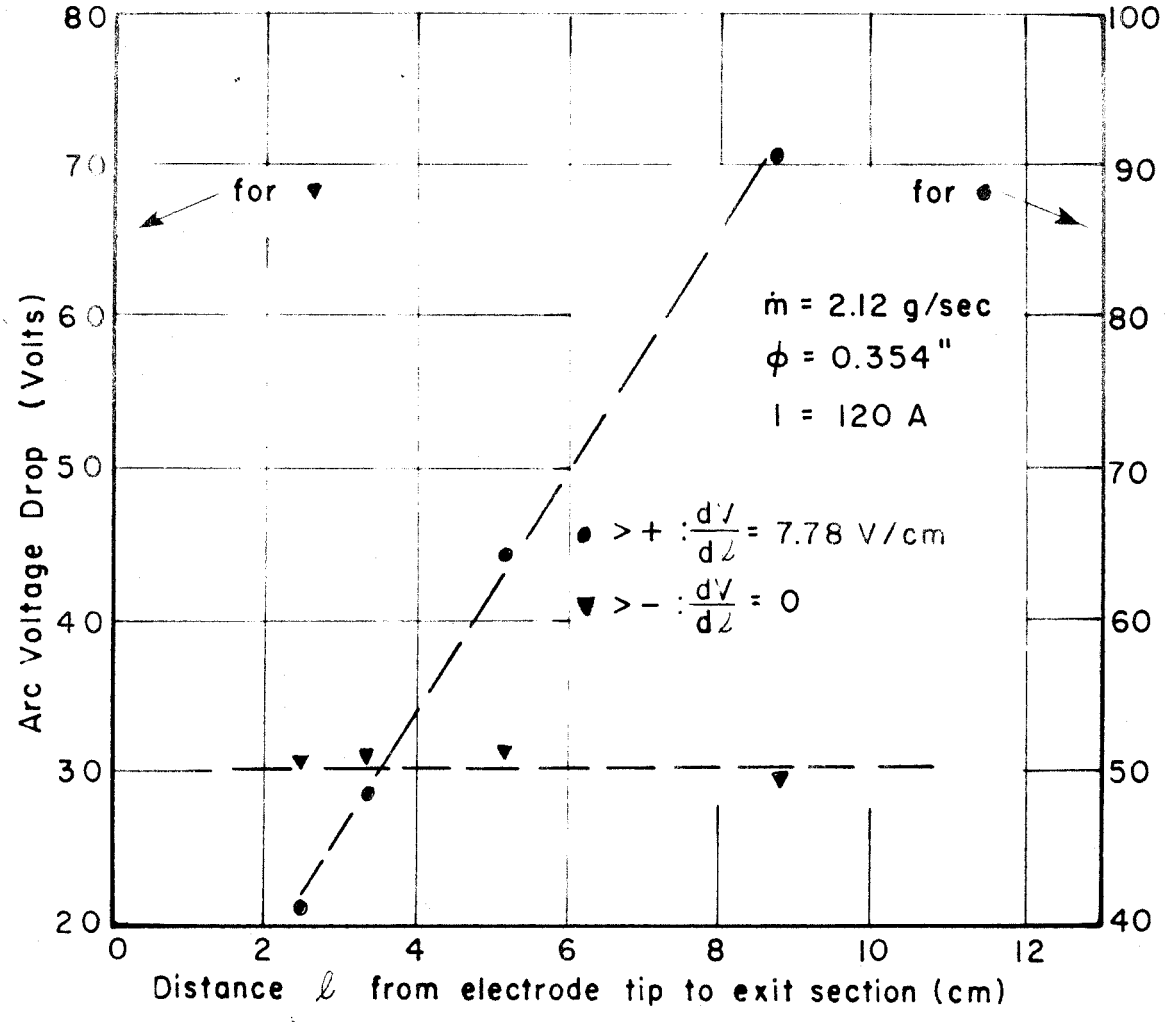

FIG. 33 ARC VOLTAGE DROP VS. DISTANCE TIP-EXIT SECTION

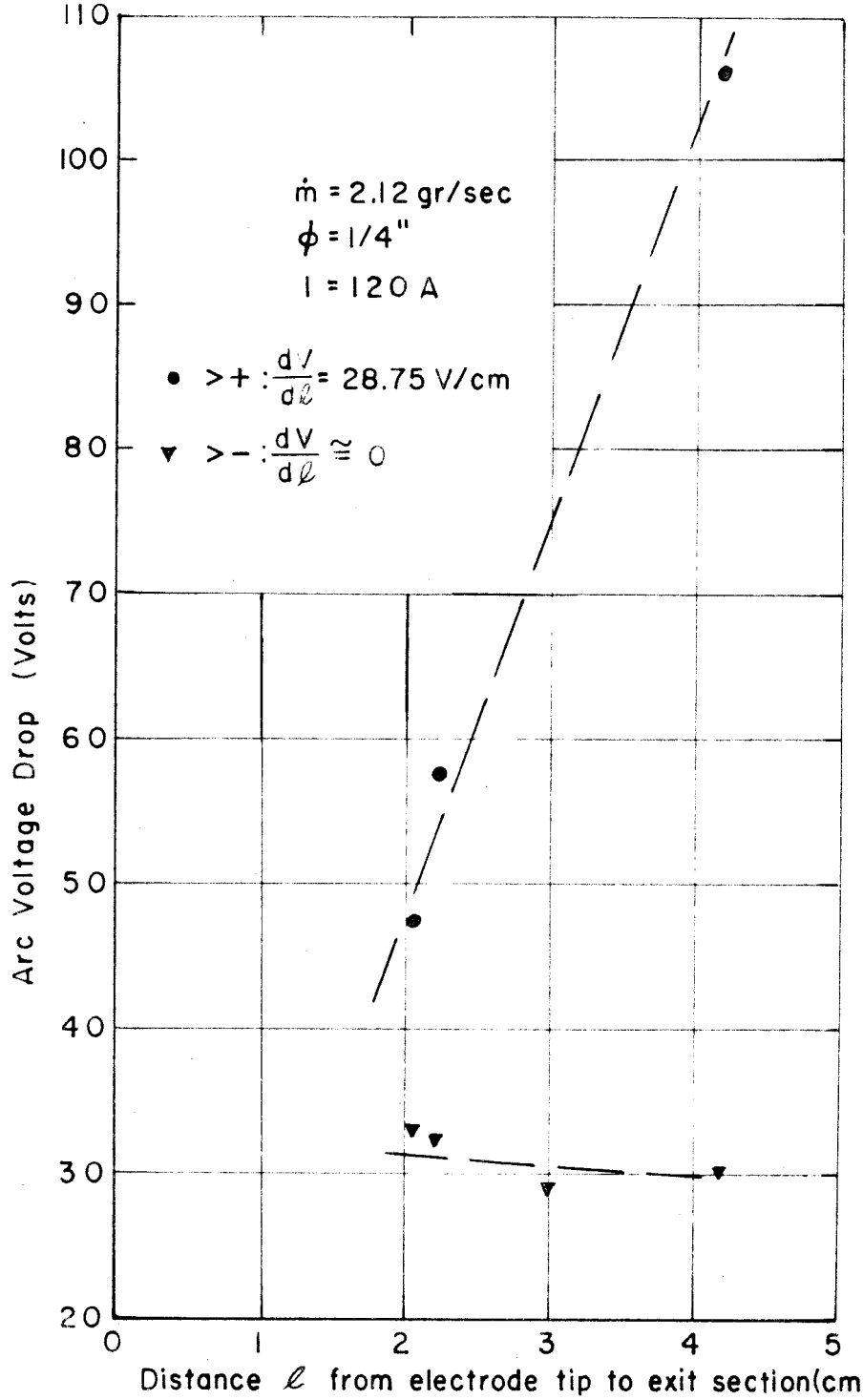

FIG. 34 ARC VOLTAGE DROP VS. DISTANCE TIP–EXIT SECTION

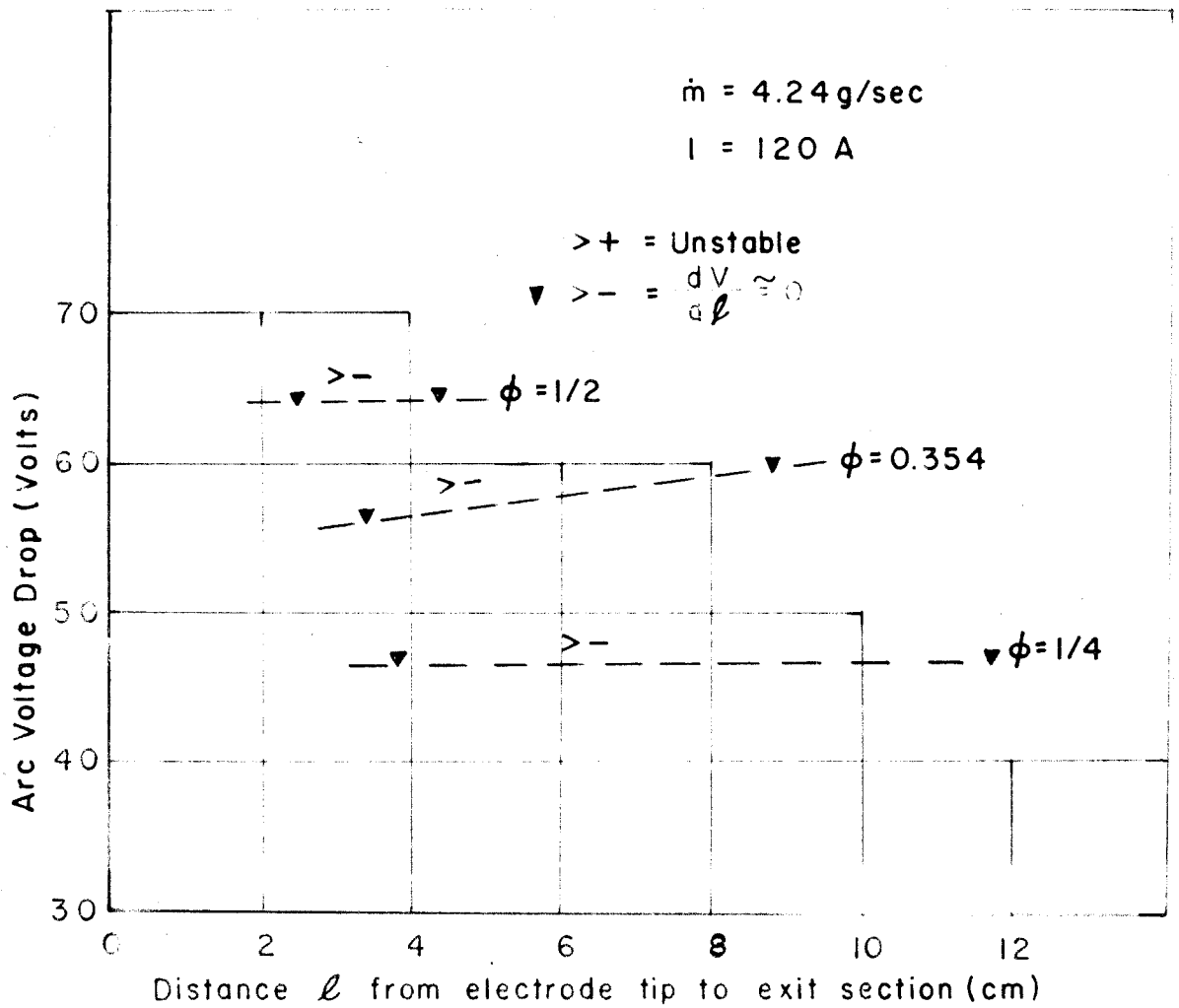

FIG. 35 ARC VOLTAGE DROP VS. DISTANCE TIP-EXIT SECTION